Sentinel User Preparation in SAR (SUPSAR)– Fundamental Scientific Developments
Theme 3: Advanced snow parameter retrieval

SUPSAR-Snow

Science Requirements

Deliverable D1

ESA Contract No: 4000148102/25/I-EB-bgh

Issue / Revision: 1/0

Date: 16 February 2026

Prepared by

Thomas Nagler, Helmut Rott

Environmental Earth Observation Information Technology GmbH (ENVEO)

Juha Lemmetyinen, Jorge Jorge Ruiz, Anna Kontu

Finnish Meteorological Institute (FMI)

Paola Rizzoli, Alexandre Becker Campos, Carolina Gonzalez

The German Aerospace Centre (DLR)

Richard Kelly, Wei Wang

University of Waterloo

Benoit Montpetit, Julien Meloche, Vincent Vionnet, Chris Derksen

Environment and Climate Change Canada (ECCC)

ILMATIETEEN LAITOS
METEOROLOGISKA INSTITUTET
FINNISH METEOROLOGICAL INSTITUTE

enveo

DLR
Microwaves and
Radar Institute

UNIVERSITY OF
WATERLOO

Environment and
Climate Change Canada
Environnement et
Changement climatique Canada

ESA STUDY CONTRACT REPORT

ESA Contract No: 4000148102/25/I-EB-bgh	Subject: Science Requirements – Deliverable D1		Contractor: FMI
ESA CR ( ) No:	Star Code:	No of volumes: 1 This is volume no: 1	Contractor's Ref: [Kategorie]

This document defines the Science Requirements (SR) and constitutes Deliverable 1 of the SUPSAR-Snow project. It provides the overarching scientific and methodological framework that guides all subsequent technical developments carried out within the project. Specifically, the document presents the key scientific objectives and questions that underpin the SUPSAR-Snow developments. It reviews the physical principles governing the interaction between synthetic aperture radar (SAR) signals and snow and summarizes the current state of the art in the retrieval of snow-related parameters from SAR observations. This review establishes a common scientific understanding and identifies existing capabilities and limitations that the project aims to address. In addition, the document consolidates the selected test areas and describes the required SAR, auxiliary, and validation datasets that support the development, calibration, and verification of algorithms for all snow parameters considered within the project. These datasets form the basis for consistent algorithm testing and performance assessment across different environmental and climatic conditions. Finally, the document defines the scientific baseline of the SUPSAR-Snow project by systematically reviewing existing retrieval and monitoring approaches for physical snow parameters derived from SAR data. For each parameter selected for further development, the current state of the art is assessed to identify gaps, challenges, and opportunities for improvement. This baseline serves as a reference against which the scientific and technical advancements achieved within the project will be measured.

The work described in this report was done under ESA Contract. Responsibility for the contents resides in the author or organisation that prepared it.

Authors: T. Nagler., H. Rott, J. Lemmetyinen, J. Jorge Ruiz, A. Kontu, P. Rizzoli, A. Becker Campos, C. Gonzalez,, R. Kelly, W. Wang, B. Montpetit, J. Meloche, V. Vionnet, C. Derksen

ESA Study Manager: Marcus Engdahl / ESRIN	ESA Budget Heading

TABLE OF CONTENTS

DOCUMENT REVISION STATUS

Last Edited Date	*Revision / Release Number*	*Status*	*Edited By*	*Pages / Paragraphs Affected*	*Change Ref*
16/2/2026	1.0 Draft		T. Nagler., H. Rott, J. Lemmetyinen, J. Jorge Ruiz, A. Kontu, P. Rizzoli, A. Becker Campos, C. Gonzalez,, R. Kelly, W. Wang, B. Montpetit, J. Meloche, V. Vionnet, C. Derksen	First version	-

APPLICABLE DOCUMENTS

AD#	*Title*	*Doc #*	*Revision*	*Date*
AD-1	Fixed Call for Proposals for Sentinel User Preparation (SUP) in SAR - Fundamental Scientific Developments (SUPSAR)	ESA CfP/5-50086/24/I-DT-bgh	1.0	29/9/2024

1. INTRODUCTION

1.1. Purpose of document

This document constitutes the Science Requirements (SR), Deliverable 1 of the SUPSAR-Snow project, and provides the high-level framework guiding all technical developments undertaken within the project.

The document outlines:

- the primary scientific questions to be addressed by the SUPSAR-Snow developments
- review of the physical background and state of the art of retrieval of snow parameters from SAR data
- consolidation of test areas together with the required SAR, auxiliary and validation datasets supporting the development, calibration and verification of algorithms for all snow-related parameters considered in the project.
- the scientific baseline for the project by reviewing the current state-of-the-art in the retrieval and monitoring of physical snow parameters from SAR observations, for each parameter selected for further development.

1.2. Structure

The report is organized into eight sections. Section 2 presents the primary objectives of the document. Section 3 reviews the state of the art in methods for retrieving physical snow parameters from SAR data, including the underlying physical principles, a review of existing algorithms, and an assessment of their limitations. Section 4 identifies gaps and challenges in current retrieval approaches and consolidates the proposed plan for algorithm development in line with the project proposal. Section 5 outlines related activities and projects of relevance for technical and scientific coordination and information exchange. Section 6 defines the test areas selected for algorithm development and demonstration, while Section 7 describes the available ground-based, airborne, and SAR datasets, together with reference data such as in situ observations. Finally, Section 8 provides the references.

1.3. Acronyms and Abbreviations

AI	Artificial Intelligence
ASCAT	Advanced Scatterometer
CPD	Co-polarized Phase Difference
CR	Corner Reflectors
DEM	Digital Elevation Model
DL	Deep Learning
DLR	Deutsches Zentrum für Luft- und Raumfahrt (German Aerospace Center)
ESA	European Space Agency
FMI-ARC	Finnish Meteorological Institute Arctic Space Centre

GEO	Geostationary/Geosynchronous Earth Orbit
GPR	Ground Penetrating Radar
IOP	Intensive observation period
LEO	Low Earth Orbit
MCh	MultiChannel
NESZ	Noise Equivalent Sigma Zero
PDF	Probability Density Function
RC	Range Compressed
ROSE-L	Radar Observing System for Europe at L-band
RVoG	Random Volume over Ground
SAR	Synthetic Aperture Radar
SD	Snow Depth
SLC	Single-look Complex
SMP	Snow Melt Phases (dry / wet / refrozen)
SoW	Statement of Work
SWE	Snow Water Equivalent
TBD	To be determined
UTC	Universal Time Coordinated
WBSCAT	Wideband microwave Scatterometer

2. PRIMARY PROJECT OBJECTIVES

The SUPSAR-Snow project aims to strengthen readiness for the upcoming Sentinel SAR Expansion and Next Generation SAR missions by advancing scientific capabilities and developing new methods for snow cover monitoring that exploit the advanced imaging characteristics of these missions. The project targets key physical snow parameters, including snow water equivalent (SWE), snow depth and snowmelt processes, and seeks to fully leverage the opportunities offered by new radar frequencies and the increased availability of SAR observations. Future missions like ROSE-L and Sentinel-1 FG/NG will facilitate the combination of C- and L-band SAR data, which is a particular focus of the project. The project also emphasizes synergy with other missions, wavelengths, and sensor types, for example in the context of the proposed Canadian TSMM mission. In addition, possibilities of bistatic measurements will be explored for retrieval of snow parameters, which are highly relevant for Sentinel companion missions such as the upcoming Earth Explorer Mission Harmony. Furthermore, the project will investigate multi-sensor data fusion approaches, including the integration of Sentinel-1 and ROSE-L observations, by exploiting the recent advances in the field of Artificial Intelligence (AI) and, in particular of Deep Learning (DL)

The following key science and technical questions are addressed in the SUPSAR-Snow project:

- Retrieval and quantification of surface melt phases (wet / dry / refrozen) from SAR data for monitoring changes for hydrology and climate research applications
- Retrieval of snow mass and snow depth from multi-frequency SAR for improved streamflow predictions and seasonal runoff forecasts, leading to improvements in flood forecasting, water management as a natural resource, hydropower and clean energy management, and advanced numerical weather predictions.

3. STATE OF THE ART FOR SAR RETRIEVAL OF PHYSICAL SNOW PARAMETERS

This section presents the state of the art in the retrieval of snow parameters from SAR data, based on a comprehensive review of scientific and technical literature, including peer-reviewed publications, project reports, and other publicly available sources. The review covers established and emerging approaches for snow parameter retrieval from SAR data and provides a structured overview of their theoretical foundations, performance, and limitations. Retrieval methods are classified according to whether they rely on SAR backscatter information or on interferometric phase–based techniques, enabling a systematic comparison of their capabilities, applicability, and sensitivity to different snow properties.

3.1. Snow Retrieval Methods based on Backscattering Intensity

Using backscatter data as input we review methods for two major physical parameters of the snowpack, namely wet snow and snow melt phases and snow mass.

3.1.1. Wet Snow and Snow Melt Phases

3.1.1.1. Physical background

The transition from dry to wet snow is accompanied by a rapid rise in dielectric permittivity (Strozzi and Mätzler, 1998), which fundamentally changes how the snowpack interacts with microwave radiation. Even small amounts of liquid water—on the order of 2% by volume—produce a strong dielectric contrast between ice and water. This contrast drastically reduces the penetration depth of C-band microwaves, bringing it close to the radar wavelength (Rott and Nagler, 1994). Whereas dry seasonal snow typically allows C-band signals to penetrate to depths of roughly 20 m, wet snow containing about 5% liquid water by volume restricts penetration to only a few centimetres (Mätzler, 1987). Figure 3.1 shows the penetration length at X-, C- and L-Band in dependence on the liquid water content. The increased permittivity and associated dielectric losses suppress transmission at the air–snow interface and enhance absorption within the snowpack. As a result, volume scattering is strongly diminished, and the dominant scattering shifts toward surface and near-surface processes.

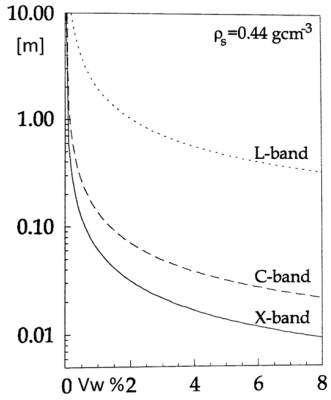

Figure 3.1: Penetration length at X- C and L- Band in dependence on liquid water content given in per cent of Volume (Vw%).

The electromagnetic changes manifest as a pronounced reduction in the backscattering coefficient (σ^o) for wet snow compared to both dry snow and snow-free ground, providing a robust physical basis for detecting snowmelt areas (e.g., Nagler and Rott, 2000; Mätzler, 1987). As liquid water content increases, σ^o decreases accordingly due to increased absorption and reduced penetration. Under wet-snow conditions, most of the radar return at L-, C- and X-band originates from the uppermost centimetres of the snowpack, whereas for dry snow, the deeper penetration means that a substantial portion of the signal originates from the snow–ground interface.

Another issue that plays a role for snow retrievals is the angular dependence of backscatter. The backscatter contrast between melting snow and snow-free surfaces changes with the local incidence angle of the radar beam, which refers to the normal surface (Figure 3.2).

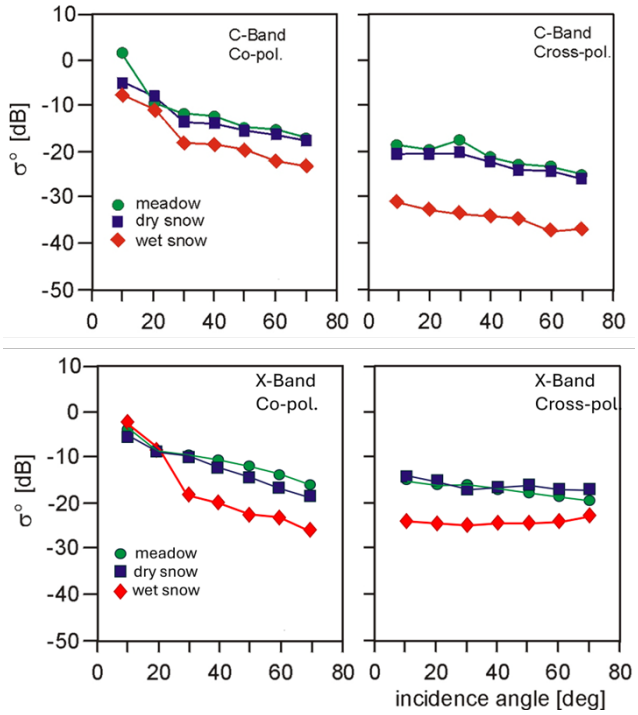

Figure 3.2: Backscatter signatures measured by groundbased scatterometer at C- and X-band, co and cross polarisation, in the test site Leutasch, Austria, for snow free, dry snow and wet snow conditions.

It is important to note that Sentinel-1, as well as most other operational SAR missions operating in the C- to X-band range, do not routinely acquire fully polarimetric data. Moreover, fully polarimetric acquisition modes are not planned for the upcoming Sentinel-1 Next Generation mission. This limits the operational use of advanced polarimetric techniques for snow monitoring using SAR data.

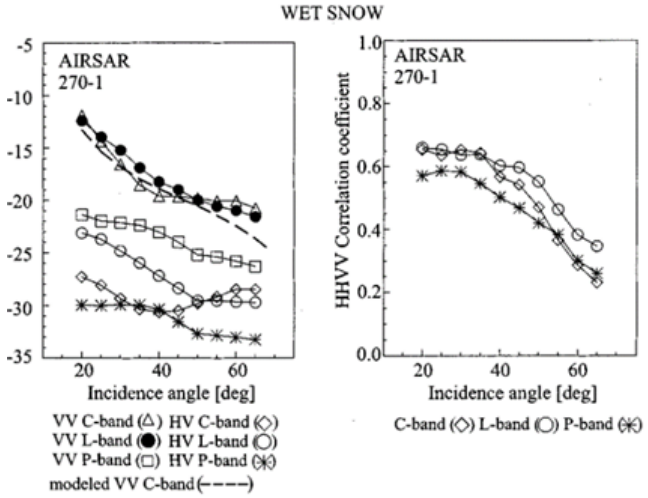

Figure 3.3: Backscatter signatures over wet snow from AIRSAR data, Ötztal, Left: σ°; right HH-VV correlation coefficient. (Floricioiu and Rott, 2001).

3.1.1.2. Algorithms for mapping wet snow

The ratio method for wet-snow mapping was first developed for detecting snowmelt in alpine regions using repeat-pass ERS C-band SAR data (Nagler, 1996; Nagler and Rott, 2000). It was later applied to a wide range of environments and sensors, including ERS observations in Scotland, Sweden, and Norway (Caves et al., 1998; Malnes et al., 2002) and adapted for agricultural areas in Québec (Baghdadi et al., 1997). The approach has also been extended to L-band (e.g., ALOS PALSAR; Solorza, 2011) and X-band sensors such as SIR-C/X-SAR, TerraSAR-X, and COSMO-SkyMed for snow mapping in mountainous terrain (Nagler, 1996; Nagler et al., 2008; Schellenberger et al., 2012).

Wet-snow detection uses a change-detection approach to distinguish snow containing liquid water from dry-snow or snow-free surfaces, relying primarily on co-polarized SAR backscatter (Nagler, 1996; Nagler and Rott, 2000) from sensors such as ERS, RADARSAT-1, and ENVISAT. The procedure comprises three main steps. First, a geocoded ratio image is generated from repeat-pass SAR acquisitions to detect backscatter changes linked to snowmelt. This involves coregistration of the snow (slave) and reference (master) images, multilooking, speckle filtering, ratio computation, and geocoding using a DEM. Layover and shadow masks, along with local incidence angle maps, are also derived from orbital geometry and DEM information.

In the second processing step, a binary snow map is derived by applying a pixel-wise threshold to the geocoded ratio image, while masking areas affected by layover, shadow, and low (<17°) or grazing (>78°) local incidence angles. Signature analyses, field observations, and comparisons with optical data indicate that a threshold of TR = –3 dB is suitable for co-polarized data (VV or HH) from ERS SAR, ENVISAT ASAR, and Radarsat SAR over alpine terrain, Scotland, Sweden, and Norway (Nagler, 1996; Nagler et al., 2000; Caves et al., 1998; Malnes et al., 2002).

The third step includes environment dependent post-processing rules, e.g. to exclude agricultural areas, open water areas, etc. (Nagler 1996; Nagler and Rott, 2004; Nagler et al., 2016).

With the launch of Sentinel-1 in 2014, routine dual-polarization SAR acquisitions over Europe enabled the development of a multi-temporal dual-pol wet-snow mapping algorithm (Nagler et al., 2016). This approach extends the original ratio method (Nagler, 1996) by exploiting the distinct incidence-angle dependencies of

co- and cross-polarized backscatter. The resulting polarization-specific ratios enhance the separability between wet snow, dry snow, and snow-free surfaces, thereby improving the robustness and reliability of wet-snow detection. Manickam and Barros et al., (2020) were adapting the method by Nagler et al., (2016) by using land surface classes as weighting factors for merging co- and cross pol backscatter data.

The Sentinel-1 baseline wet-snow products exhibit a high level of consistency, demonstrating overall agreement rates of 95% or greater when compared with high-resolution snow products derived from Landsat data across multiple test sites in the Alps and Iceland during melt conditions. Karbou et al. (2022) used this product for deriving the snow line for mountain ranges in the Alps during the melting period in the Alps and reports a good agreement with Sentinel-2 products. The dual-pol Sentinel-1 algorithm by Nagler et al. (2016) is the basis for the wet snow products generated from Sentinel-1 within the Copernicus High Resolution Water Snow and Ice Service, funded by the European Environment Agency EEA (Copernicus Land Monitoring Service web site https://land.copernicus.eu).

3.1.1.3. Methods for monitoring Snow Surface Melt / Refreeze

The physical basis for generating high resolution maps of snow melt extent, accounting for different melting phases (dry snow, wet snow, refrozen snow surface on top of wet snow) from C-band backscatter measurements was studied in the AlpSnow project for Alpine regions (AlpSnow D3.2/2 ATBD v2, 2023). The snow melt phase product is an extension of the wet snow mapping procedure described in the previous section and analyses the evolution of the backscatter time series.

The sensitivity to refreezing of wet snow increases with decreasing wavelength. At X-band the refrozen snow grains and grain clusters are efficient scatterers. The Shuttle Radar Experiment data on Rofental Glaciers show an increase of σ°(X-VV) of 8 dB within 4 days due to refreezing of wet snow in the accumulation areas in early autumn (Floricioiu and Rott, 2001). X-band (10.4 GHz) backscatter measurements of night-time refreezing at Weissfluhjoch show σ° increase of up to 5 dB within a single night (Reber et al., 1987). These observations confirm the relevance of X-band data for the observation of melt-freeze cycles. At C-band the impact of the refrozen crust is less strong. Backscatter simulations reveal an increase of up to 3 to 4 dB for a surface crust with 10 cm thickness depending on the grainsize and clusters of the refrozen crust (AlpSnow D3.2/2 ATBD, 2023).

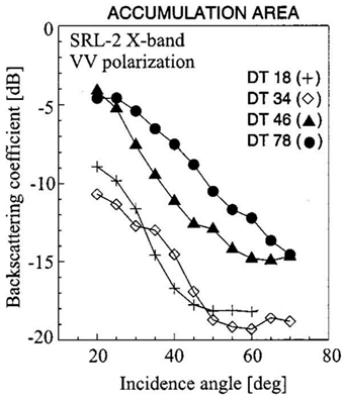

Figure 3.4: Backscatter increase (X-band VV) due to refreezing crust on top of wet snow on Rofental glaciers, SRL-2, 1 Oct. 1994 (DT18) to 5 Oct. 1994 (DT78) (Floricioiu and Rott, 2001).

Within AlpSnow, dense Sentinel-1 time series were analysed to assess the mission's capability to monitor the melt–refreeze cycle of the seasonal snowpack during the main melt period. Based on the temporal evolution of C-band backscatter in repeat-pass acquisitions, three characteristic phases were identified on a pixel-by-pixel basis. With Sentinel-1A and 1B, 6-day repeat pass SAR data were available, following the loss of Sentinel-1B in December 2021, the repeat interval increased to 12 days. This temporal sampling allows characterization of early- and late-season melt dynamics in the Alps. However, detecting individual melt–refreeze events requires same-day observations from ascending (afternoon) and descending (morning) orbits. Over the Alps, such paired acquisitions are available only at multi-day intervals. Systematic monitoring of melt–refreeze events therefore requires more frequent—ideally daily or sub-daily—SAR observations, as they could be provided by EE12 Candidate Mission Hydroterra+. For testing the approach ground-based observations with continuous observations every few hours are useful. Although such data sets are currently not acquired by spaceborne SAR systems, ground-based systems will provide the high sub-daily observations to develop and test methods for detecting surface crust formation.

3.1.1.4. Mapping of snow melt phases and surface refreezing depth for polar ice sheets and ice shelves

The melt and refreeze conditions of ice sheet surfaces are basic information for modelling the meltwater volume, surface runoff and surface energy budget. Data on surface meltwater production and presence are also crucial for estimating changes in the subglacial water pressure, a main parameter for glacier speed-up. The melt dynamics play an important role for the stability of ice sheets and ice shelves, as the amplification of surface melting as precursor to glacier speed-up in Greenland and the collapse of ice shelves on the Antarctic Peninsula have shown. Based on Scatterometer and SAR data Nagler et al. (2024) proposed a procedure to map surface melt phases for ice sheets and ice shelves by timeseries analysis of ASCAT and Sentinel-1 data. Three surface melt phases are discriminated, (i) dry, (ii) wet surface layer, (iii) refrozen surface layer on top of wet snow. Figure 3.5 shows the time series of Sentinel-1 A and 1B backscatter at the Larsen Iceshelf, Antarctic Peninsula. Short-term melting of a thin surface layer is observed in November and May, indicated by a decrease in backscatter, followed by complete refreezing of the melted layer by the next observation. In January, surface-layer melting is more pronounced, as evidenced by a strong decrease in backscatter, and refreezing occurs over a period of several weeks.

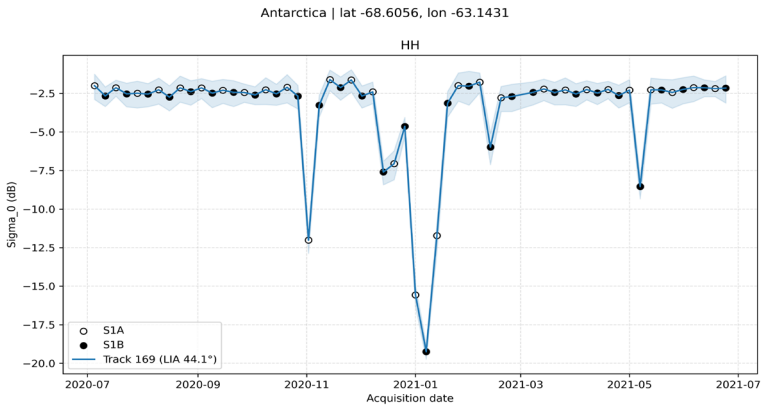

Figure 3.5: Sentinel-1 C-Band HH backscatter timeseries, Larsen Shelf Ice, Antarctica. Melt of a thin surface layer is observed in November 2020 and May 2021, in January 2021 full melt is observed, refreezing is indicated by the increase of backscatter end of January.

Due to the strong dielectric losses of liquid water, the penetration depth of C-band microwaves in wet snow is limited, causing the backscatter signal to saturate once the surface melt layer reaches a moderate thickness. On the other hand, wet snow below a refrozen surface layer can be detected down to larger depth (Figure 3.6). The algorithm for identifying different melt stages exploits both the attenuation of the backscatter signal within the wet snow layer and the vertical position and extent of this layer within the firn column (Nagler et al., 2024). Figure 3.7 illustrates a C-band backscatter simulation for wet snow surfaces with liquid water contents ranging from 1%^{vol} to 5%^{vol}, as well as for a refrozen surface layer overlying wet snow. Owing to the strong absorption by liquid water, the C-Band backscatter from wet snow saturates rapidly (Figure 3.7). The backscatter simulations assume homogeneous layers with a density of 400 kg m^{-3} and spatially uniform wetness. In a wet snow layer, the C-band signal saturates at a total liquid water content of only a few millimetres and has a maximum sensing depth of several decimetres, limiting its suitability for quantitative wetness retrievals Figure 3.7a). The temporal evolution of the signal during refreezing, however, exhibits a substantially larger sensing depth (Figure 3.7b). The sensitivity of the C-band backscatter change to the refreezing depth decreases as the refrozen layer thickens.

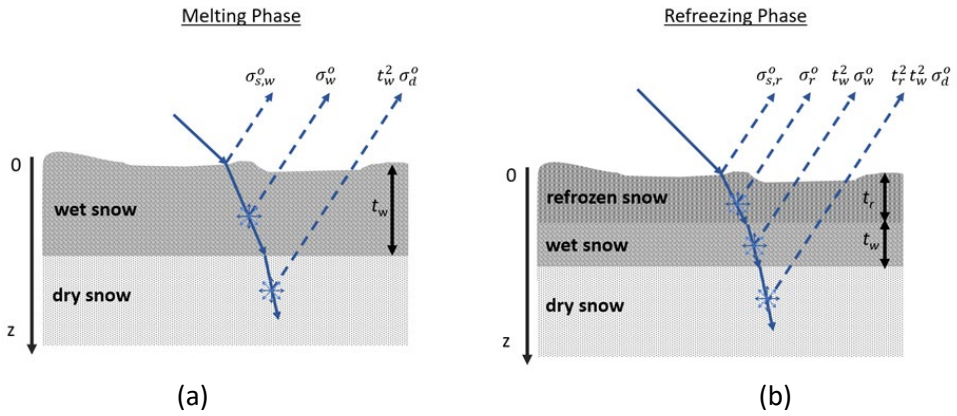

Figure 3.6: Main backscatter contributions from snow volumes with (a) wet surface layer and (b) refrozen layer on top.

Nagler et al (2024) developed a method for monitoring surface melt and refreeze phases on ice sheets, exploiting dense time series of C-Band backscatter data from spaceborne active microwave sensors. The procedure was applied to ASCAT SIR products with 4.45 km pixel spacing to observe the evolution of the surface melt and refreeze on the Greenland and Antarctic ice sheets but was tested only for a few Sentinel-1 C data, which would provide much higher resolution suitable for complex terrain such as outlet glaciers on the Antarctic Peninsula.

The depth of the refrozen surface layer is a new product, which provides detailed insights into the melt–refreeze cycle on ice sheets, supporting studies and modelling of surface processes as well as the quantification of surface melt. At C-Band the backscatter signal saturates already a about 1 m thickness of the refrozen layer (Figure 3.7b). The integration of C- and L-Band will provide a more robust estimation of the refrozen layer, but close acquisition of both frequencies is needed.

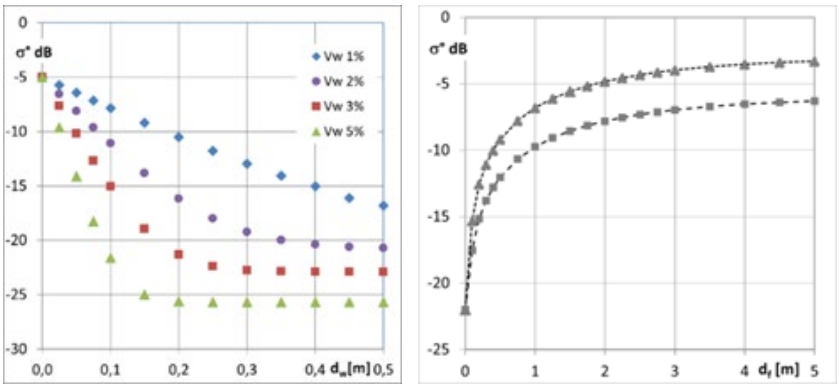

(a) (b)

Figure 3.7: (a) Simulation of C-band backscatter coefficient, VV polarization (θ_i = 30°), for a wet snow layer of depth d_w with volumetric water content V_w = 1, 2, 3, 5 $\%^{vol}$, above a semi-infinite dry snow/firn layer. (b) Simulation of C-band backscatter coefficient (θ_i = 30°) of a refreezing snow and firn layer of thickness d_f above an opaque layer of wet snow and firn with σ° = -22 dB. For the refrozen layer two volume scattering cases are assumed, corresponding in the semi-infinite case to σ° = -3 dB (▲) and σ° = -6 dB (■).

3.1.2.Snow Water Equivalent from backscatter data

High frequency radar observations have been proposed as a potential tool to retrieve Snow Water Equivalent. This section describes the physical basis of the approach, summarizes recent field work and development in forward models and retrieval algorithms.

3.1.2.1. Physical background

The method for detecting snow mass using radar assumes that an increasing amount of snow will induce increased volume scattering from the snow medium, observed as an increase in backscattering intensity, when observed at an optimal wavelength. In passive microwave remote sensing, the same principle is exploited from the point of view of observing increasing extinction in the snow with increasing snow mass.

For the radar case, the total backscatter σ_{pq}^t observed from a snow-covered surface by a monostatic radar can be considered to consist of several components so that

$$\sigma_{pq}^t = \sigma_{pq}^s + \sigma_{pq}^v + \sigma_{pq}^g \exp\left(-2\tau \sec\theta_t\right)$$

where σ_{pq}^s is scattering from the snow surface, σ_{pq}^v is scattering from the snow volume, and σ_{pq}^g is scattering from the ground surface, attenuated by a two-way extinction term (Tsang et al., 2022). Figure 3.8 shows a sketch of the scattering components.

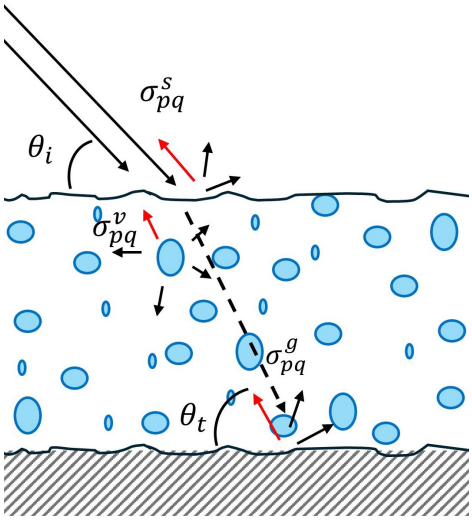

Figure 3.8: Scattering components from snow-covered surfaces.

For dry snow, scattering from the snow surface (σ_{pq}^{s}) can typically be considered minimal. The interaction of electromagnetic waves with the snow volume depends on the snow properties, the frequency and polarization of the waves. To derive volumetric properties such as snow mass, the chosen frequency should penetrate the snowpack while still interacting with the snow medium sufficiently to provide a backscattering signal (σ_{pq}^{v}) from the snow volume. A critical factor here is the size of snow particles ('snow grains') compared to the wavelength; longer wavelengths (low frequencies, C-band and below) where the wavelength is in the order of several centimeters or more, will largely penetrate a dry snowpack and the main backscattering contribution will originate from the background (σ_{pq}^{g}) attenuated by the snow. For wet snow and for higher frequencies, the surface scattering term (σ_{pq}^{s}) becomes the dominant source of scattering.

Higher frequencies such as X (8-10 GHz) and Ku-band (12-18 GHz) have a wavelength proportional to the snow microstructure and should, from the theoretical point of view, experience increasing volume scatter with increasing frequency and increasingly coarse microstructure (Zhu et al., 2018). For e.g. Ka-band, scattering should already be strong, and the penetration of the radar signal limited to a few centimetres for coarse-grained snow. Table 3.1 summarizes generalized behaviour of different wavelengths.

Table 3.1:

Generalized radar backscattering response to dry seasonal snow cover from C- to Ka-bands.

Frequency	*Typical 2-way penetration depth*		*Comments / Sensitivity*
	Fine-grained snow	Coarse snow (depth hoar, melt/freeze)	
Ka (35 GHz)	≤ 0.5 m	few cm	Mainly sensitive to micro-structure of top snow layer.
Ku (17 GHz)	≤ 2 m	≤ ca. 20 cm	Low sensitivity to fresh, fine grained snow. Possible saturation for deep coarse-grained snow layers.
Ku (13.5 GHz)	≤ 3 m	≤ ca. 50 cm	Low sensitivity to fine-grained snow.
X (10 GHz)	≤ 10 m	≤ ca. 1 m	Very low sensitivity to snow with fine to medium sized grains. Sensitivity for deeper snowpacks and coarse-grained snow.
C (5 GHz)	≤ 20 m	≤ ca. 5 m	Backscatter signal from ground surface below dry snow dominates. Ratio of co- and cross-polarized backscatter has been proposed for retrieval of deep snow (> 1.5 m)

Already early theoretical simulations identified a response to SWE at Ku-band (Ulaby and Stiles, 1980). These findings were initially supported by airborne Ku-band measurements from the NASA Cold Land Processes Experiment (CLPX; Yueh et al., 2009). Exploiting these findings, several mission proposals have been submitted to space Agencies for retrieving snow properties with high-resolution SAR. Notably, the Cold Regions High Resolution Hydrological Observatory (CoReH2O) was proposed as a mission candidate for the ESA Earth Explorer 7 (Rott et al., 2010). CoReH2O proposed a combination of an X- and Ku-band SAR to derive Snow Water Equivalent and snow accumulation on glaciers at high spatial resolution, every 3 or 15 days depending on the mission Phase. The frequency combination was thought to be optimal for sensing both fine-grained boreal & taiga snowpacks and deep snowpacks in Alpine areas.

The Canadian Space Agency (CSA) is currently considering a concept study, the Terrestrial Snow Mass Mission (TSMM), proposing a dual Ku-band scatterometer to derive SWE (Derksen et al., 2021). Evolved from the CoreH2O mission proposal, the mission would be the first spaceborne Ku-band SAR mission of its kind. The concept also plans to use C-band SAR, Radarsat Constellation Mission over Canada and Sentinel-1 over Europe, to decouple the backscattered signal of the snow from the underlaying ground and improve the accuracy of SWE retrievals (Montpetit et al., 2024).

3.1.2.2. Forward models and retrieval algorithms for SWE

Tsang et al. (2022) provide a review of retrieval algorithm development since CoReH2O, highlighting advancements in both forward modelling and retrieval approaches. In forward model developments, Proksch et al. (2015) presented an active microwave version of the Microwave Emission Model for Layered Snowpacks (MEMLS). SnowScat observations from the NoSREx campaign were applied for validating model simulations at X- and Ku bands. Chang et al. (2015) applied the same observations for comparisons of backscattering estimates using two derivations of the dense media radiative transfer (DMRT), the bicontinuous model and quasi-crystalline approximations (QCAs). Both approaches showed reasonable agreement with SnowScat observations collected during the second campaign season. Furthermore, Tan et al. (2015) demonstrated the necessity of multiple scattering enhancement in DMRT, using both active and passive observations from NoSREx for model evaluation.

The review paper by Tsang et al. (2022) highlights four different approaches (Lemmetyinen et al., 2018; King et al., 2019; Thompson and Kelly, 2021; Zhu et al., 2018) of which the one by Zhu et al. (2018) is presented in more detail; the authors propose a radar-only SWE retrieval method that uses a physically based bi-continuous Dense Media Radiative Transfer (DMRT) model, but simplifies its inversion so it can be applied operationally with X/Ku-band radar. The method first subtracts the ground-surface backscatter (estimated from snow-free data or DMRT simulations) to isolate the snow volume-scattering signal. Using DMRT, the authors build extensive lookup tables and then apply regression algorithms to compress the snow scattering physics into two effective parameters—albedo (ω) and optical thickness (τ). The algorithm then performs a two-channel inversion (typically X- and Ku-band co-pol σ^o) to solve for ω and τ, after first classifying the snowpack into low- or high-albedo regimes to reduce ambiguity. Finally, SWE is retrieved using a simple empirical relation linking SWE to $(1 - \omega)\tau$, calibrated from DMRT simulations and validation datasets. The result is a compact, physically guided SWE retrieval that avoids the full complexity of DMRT forward modelling during inversion.

Recently, Pan et al. (2024) adapted the MEMLS3&a(Proksch et al., 2015) forward model within a Bayesian MCMC framework, using minimal, uninformed prior constraints on snow microstructure, to jointly retrieve snowpack parameters (including SWE, layering, density) and surface properties from three-frequency (X + dual Ku) radar backscatter. The method was applied to the NoSREx dataset. The results (Figure 3.9) suggest that the method can potentially improve SWE and snow-depth retrieval accuracy over simple prior-based estimates.

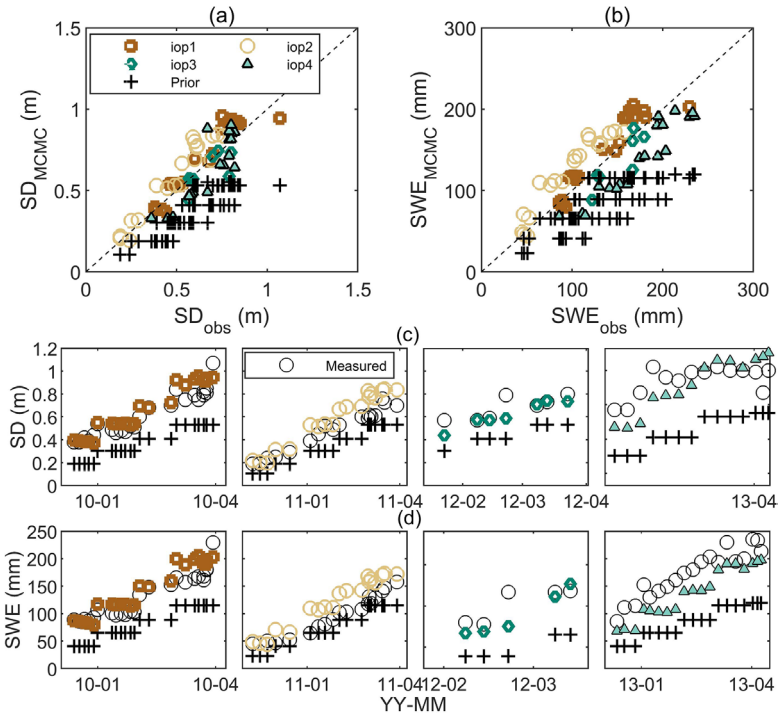

Figure 3.9: Estimated snow depth (SD, a, c) and SWE (b, d) using a Bayesian Markov Chain Monte Carlo method versus observations at Sodankylä during the NoSREx experiment. Scatterplots are shown in (a) and (b), and the time series are shown in (c) and (d). Pan et al., 2024.

3.2. Snow Retrieval Methods using Interferometric Phase data

The interferometric SAR (InSAR) phase provides sensitive information on changes of snow parameters. We separate repeat-pass InSAR (RP-INSAR) and single-pass InSAR (SP-InSAR) methods.

3.2.1.ΔSWE Retrieval using Repeat-Pass InSAR

Changes in SWE (ΔSWE) can be calculated using repeat-pass differential Interferometric SAR (Guneriussen et al. 2001; Rott et al., 2003, Nagler et al., 2022), for dry snow conditions. Since dry snow has a higher real permittivity than air, its presence induces an increase in the optical path of the microwaves. Furthermore, absorption for dry snow (imaginary part of the permittivity) is low for frequencies below 18 GHz. Therefore, the difference in the snow conditions (e.g., its presence or accumulation) between two SAR acquisitions separated in time will induce differences in the phase that can be linked to ΔSWE. Figure 3.10 illustrates the method. The method has been demonstrated using tower-based radar (Leinss et al., 2015; Jorge-Ruiz et al., 2022), airborne (Hoppinen et al., 2024, Nagler et al., 2022, Nagler et al., 2024a), and spaceborne datasets (Oveisgharan et al., 2024, Jorge-Ruiz et al., 2024, Nagler et al., 2022, Nagler et al. 2024b).

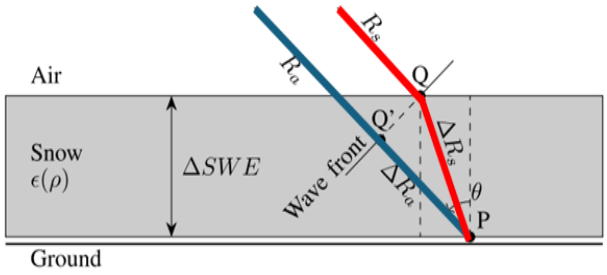

Figure 3.10: Illustration of the method for ΔSWE using repeat-pass InSAR. The difference in the travel distance between the snow scenario (red line) and the snow-free scenario (blue line), can be linked to changes in ΔSWE.

Tower-based experiments have demonstrated the retrieval for frequencies between 1 and 18 GHz, leveraging short temporal baselines between 4 and 12 hours, to reduce temporal decorrelation (Leinss et al., 2015; Jorge-Ruiz et al., 2022). These studies also analysed the meteorological effects leading to temporal decorrelation in snow, suggesting that air temperatures above 0°C are what environmental effects lead temporal decorrelation in snow, suggesting that the presence of liquid water in the snowpack has a significant impact on SAR signal. Airborne investigations have validated the method across multiple frequency bands (L- and C-band), diverse topographic settings, and varying snow regimes (Hoppinen et al., 2024; Nagler et al., 2022; Palomäki et al., 2023; Bonnell et al., 2024). These studies investigated how topography, vegetation, and snow cover impact the retrieval performance, often using extensive ancillary datasets, such as Ground Penetrating Radar (GPR), LiDAR, and snow course measurements, to support the analysis. Finally, studies using satellite imagery have demonstrated the technique over extended areas. In Jorge-Ruiz et al., (2024), L-band ALOS2 imagery with 14 days temporal baseline was used against snow simulations from SnowModel, and the effect of the vegetation in the retrieval analysed. Results indicate that retrievals over vegetation are affected by air temperatures, since vegetation's transmissivity increases for freezing temperatures. The first season-long retrieval of ΔSWE was presented in Oveisgharan et al., (2024), where in-situ snow stations were used to calibrate the interferometric phase. Figure 3.11 presents the cumulative or total SWE over two areas

was compared to LiDAR measurements, showing moderate agreement between them. An improvement to the calibration method was proposed in Zhou et al. (2025), exploiting connected networks of interferograms. A comparison between frequency bands, and possible combinations of them was proposed in Belinska et al., 2023, highlighting some of the limitations of the technique with respect to lost phase cycles.

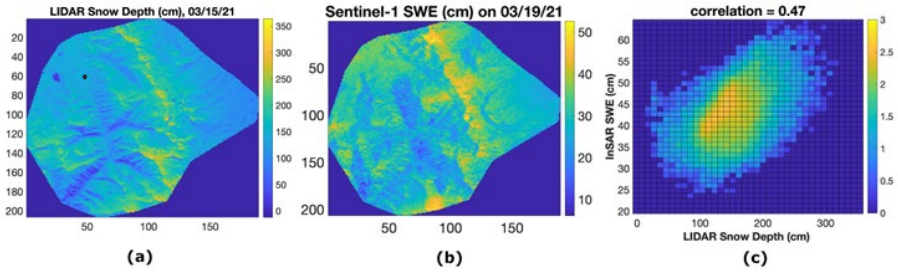

Figure 3.11: Comparison of LiDAR snow depth and cumulative SWE derived from Sentinel-1 InSAR time series over Banner Summit, Idaho, during mid-March 2021, presented in Oveisgharan et al., (2024). (a) LIDAR snow depth in cm, (b) Sentinel-1 SWE in cm, and (c) 2D histogram between data from (a) and (b).

3.2.1.1. Challenges of RP-INSAR ΔSWE retrieval

Temporal decorrelation of the InSAR signal is the primary limitation of the method and is driven by changes in snow properties such as structure, liquid water content, and surface roughness. The underlying model assumes sufficient radar penetration into the snowpack, with the effective phase center located at the snow–ground interface, allowing interferometric phase variations to be related to changes in snow depth or snow water equivalent. Accordingly, the method has mainly been applied using radar systems operating between 1 and 10 GHz, where penetration into dry snow can be expected. However, retrieval accuracy is strongly reduced by temporal decorrelation and loss of phase coherence, which are particularly pronounced during strong snowfall events and snow redistribution by wind drift. These effects increase with higher frequencies and rapidly evolving snow conditions. To mitigate these limitations, lower-frequency radar bands such as L-band, and in some cases C-band, are generally preferred due to their improved temporal coherence and greater penetration depth, despite trade-offs in sensitivity that must be considered depending on the application (Luzi et al., 2009; Nagler et al., 2022, 2024; Jorge-Ruiz et al., 2022; Belinska et al., 2023; Benedikter et al., 2024).

Snowmelt represents another major source of decorrelation, as the presence of liquid water rapidly destroys signal coherence (Rott et al., 2003, Jorge-Ruiz et al., 2022). Consequently, areas affected by snowmelt should be masked using wet-snow detection approaches, for example based on changes in radar backscatter.

Another challenge of the method is the high sensitivity of the interferometric phase to snow accumulation, which can cause the phase change to exceed the unambiguous range of 2π. This effect is more pronounced at higher frequencies due to their shorter wavelengths. For example, at C-band, assuming an incidence angle of 22.5° and a snow density of 0.2 kg m^{-3}, a full phase cycle corresponds to approximately 31 mm of snow accumulation, which can occur within typical SAR revisit intervals of 6 to 14 days. In contrast, under the same conditions, the unambiguous retrieval range at L-band increases to approximately 120 mm, substantially reducing the likelihood of phase wrapping errors (Figure 3.12).

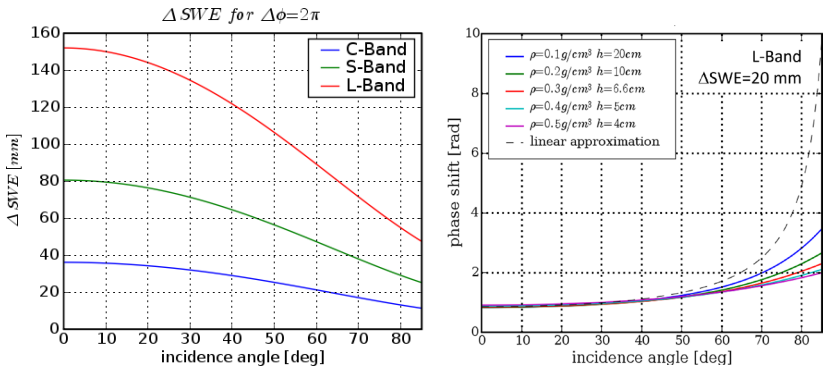

Figure 3.12: ΔSWE for a phase cycle of 2P for L- (24 cm wavelength), S- (13 cm) C- (5.6 cm) band in dependence on the local incidence angle. (b) Interferometric phase shift $\Delta\phi$ at L-band calculated for ΔSWE = 20 cm, at for different snow densities between 0.1 and 0.5 g cm^{-1}.

Selection of references for InSAR derived ΔSWE, can be complicated, as scenes may lack snow-free pixels, targets with stable phase behaviour (e.g. buildings of Corner Reflectors, CR), or in-situ measurements. In the present literature, all these methods have been used, but it's application over remote areas may be limited (Oveisgharan et al., 2024; Belinska et al., 2023; Jorge-Ruiz et al., 2022, Palomaki et al., 2023). Selecting a suitable reference point for the retrieval can be difficult, since some remote areas lack a known ground point (e.g., a snow station). Some images may lack a snow-free area that could be use as reference, as the whole image may be covered by snow.

Another limitation is the presence of vegetation, which in many areas of the world (such as Lapland) dominates the landscape. Vegetation also affects the retrievals, with increasing effect for higher frequency bands, by inducing an additional phase component and increasing decorrelation (both volume and temporal). Studies have shown that L-band can effectively penetrate through the vegetation structure and effectively retrieve ΔSWE, even with the model presented in Guneriussen et al. 2001, thus assuming that the error induced from the vegetation is small. Jorge-Ruiz et al., 2024 proposed that this can only be applied when the air temperature is sufficiently low, as the vegetation complex permittivity decreases in freezing conditions (Lemmetyinen et al., 2022). Although the technique has been applied over forested areas with no additional modifications to the basic method (Jorge-Ruiz et al., 2024, Bonnell et al., 2024), the results for the retrieval depend on environmental conditions, with increasing error for close to 0C temperatures. Additional modelling of the wave interaction with the vegetation can compensate the additional phase component. A modification based on the well-known Random Volume over Ground (RVoG) model has been proposed, but it has not been widely validated (Lei et al., 2023).

The utilization of multiple frequency bands has been proposed in order to reduce uncertainties derived from low coherence and lost phase cycles. Leinss et al., 2015 proposed joint utilization of Ku-low and Ku-low to recover lost phase cycles, but its parametrization does not depend on interferometric observables. Belinska et al., 2023 investigated the utilization of non-coincidental InSAR images to recover lost phase cycles, but the method assumes a constant increase of SWE over time, which does not reflect common accumulation patterns. MultiChannel (MCh) techniques emerge as a solution not only to recover lost phase cycles but also mitigate noise in the estimation (Baselice et al., 2015). By exploiting the Probability Density Functions (PDFs) of coincidental and statistically independent InSAR acquisitions, some uncertainties inherent in InSAR estimation can be mitigated. Using L–S, L–C, and C–X band combinations from a tower-based radar system,

Jorge-Ruiz et al. (in preparation) achieved $R^2 > 0.8$ for ΔSWE over temporal baselines of up to 80 days, when validated against an in-situ snow scale.

Compensating for the Atmospheric Phase Screening (APS) is also required. In particular, L-band is heavily affected by the ionosphere. While some methods to compensate for it have been proposed (such as the split spectrum method, Liang et al., 2017), these depend on unwrapping the phase from the sub band interferograms. This is prone to fail in low coherence scenarios, such as are common in snow covered terrain. Alternatives relying from external sources (not dependent on the InSAR image quality), such as GACOS (Xiao et al., 2021), present an interesting alternative.

3.2.2. Snow Depth Retrieval using Single-Pass InSAR

This section reviews methods for retrieving changes in snow depth by differencing digital elevation models (DEMs) acquired before and after snowfall events. The approach relies on the accurate generation of surface DEMs (also called Digital Surface Models (DSM)), typically derived from SAR interferometry or other remote sensing techniques, and assumes that elevation changes between acquisitions are primarily driven by snow accumulation or ablation. Key aspects discussed include DEM accuracy requirements, sources of uncertainty such as surface roughness and vegetation, and the temporal and spatial constraints that affect the reliability of snow depth change estimates.

In situ snow depth can be measured through manual probing or automated ultrasonic sensors, but such point measurements are highly sensitive to local effects related to elevation, topography, vegetation, and wind redistribution. As a result, they are typically not representative of spatially extensive snow conditions. Remote sensing approaches operating in the optical and microwave domains address this limitation by enabling snow depth estimation across larger regions. Among these methods, single-pass InSAR enables a robust framework for snow depth retrieval by exploiting the interferometric phase generated from two SAR images acquired simultaneously by spatially separated antennas. This configuration avoids the presence of temporal decorrelation and atmospheric phase screen variability that can affect repeat-pass interferometry -- which is particularly important given the rapid change of snowpack properties through accumulation, metamorphism and melt -- and enables meter-scale spatial resolution and sub-meter to centimeter-scale vertical accuracy Digital Elevation Models (DEMs).

In this context, a widely used implementation of single-pass InSAR for snow depth estimation relies on DEM differencing, where the measured InSAR DEM elevation $h_{InSAR,\,snow}$ is compared with a snow-free reference elevation, $h_{snow-free}$, derived from LiDAR, photogrammetry, or earlier SAR acquisitions:

$$\Delta z_s = h_{\text{InSAR, snow}} - h_{\text{snow-free.}}$$

This formulation has been applied extensively in recent years for snow depth retrieval using a variety of single-pass InSAR systems. For example, Moller et al., 2017 demonstrated the effectiveness of the airborne Ka-band GLISTIN system in the Tuolumne River Basin, where wet-snow depth maps showed a standard deviation below 1 m, with the largest discrepancies occurring on steep slopes. Similarly, Leinss et al., 2018 applied single-pass DEM differencing to TanDEM-X acquisitions in northern Finland, confirming that the approach is operationally attractive for wet-snow conditions, although its accuracy remains dependent on precise co-registration, low noise-equivalent sigma0 (NESZ), and high-quality reference DEMs. In particular, the bistatic TanDEM-X system (Krieger et al., 2007), launched in 2010 and operational to this day, has been

widely employed to estimate relative snow depth and glacier height changes using DEM differencing. Numerous glaciological studies have exploited TanDEM-X DEM pairs for glacier mass-balance and elevation-change assessments (e.g., Braun et al., 2019; Sommer et al., 2020; Rankl et al., 2016). An intrinsic limitation of such approaches is the penetration of the radar wave into the snow. While Ka-band systems such as GLISTIN typically show limited penetration depths of approximately 0.3–1 m in dry firn on the Greenland Ice Sheet (Hensley et al., 2016), the X-band TanDEM-X system can experience penetration biases of several meters under dry-firn conditions (Becker Campos et al., 2025a). The penetration depth of the radar signal depends on different factors, such as the sensor frequency, the acquisition geometry, and the snowpack characteristics (e.g., snow grain size, density, and liquid water content) (Rignot et al.,1993). In the presence of penetration, the interferometric phase center of the backscattered radar signal is positioned below the actual surface, resulting in a bias relative to the surface which can be particularly significant over dry snow, where the absence of liquid water and the homogeneity of the medium exacerbates penetration effects to potentially several meters, depending on the radar wavelength.

Benedikter et al., 2023 showed that the relationship between the true surface height $h_{surface}$ and the apparent phase center height measured with conventionally processed InSAR h_{InSAR} can be approximated as

$$h_{\text{surface, snow}} = h_{\text{InSAR}} + \Delta h - \Delta h_2$$

where Δh is the physical penetration bias (assumed positive) and Δh_2 (assumed negative for biases oriented downward) is the propagation bias, which may be quantified by evaluating the change in the interferometric vertical wavenumber when propagating into the firn volume, as the vertical wavenumber is stretched when penetrating in the dielectric denser medium. Figure 3.13 illustrates this relationship. Therefore, a bias correction step to be applied to the InSAR DEM, either through physical-based radiative transfer models (Weber Hoen and Zebker, 2000) or through data-driven approaches such as deep learning (Becker Campos et al., 2025a), is required to accurately estimate snow depth from InSAR measurements affected by penetration.

When working with InSAR-derived DEMs, it is important to account for residual offsets and tilts resulting from uncertainties in the estimation of the normal baseline. These effects must be properly corrected before performing DEM differencing to ensure reliable retrieval of elevation and snow depth changes (Krieger et al., 2007). For example, regarding TanDEM-X, an error in the baseline estimation in the order of 1 mm leads to a height error in the resulting DEM in the order of 1 m. Therefore, the order of magnitude of residual offsets and tilts is comparable to the quantity to be estimated, i.e. the snow depth, making their compensation of paramount importance for archiving reliable results. This residual mutual calibration of DEMs is in general performed by utilizing reference tie-points, whose location and height is known a priori, or estimated through other reference sensors, such as GPS or LiDAR data. The manual procedure is time-consuming and can be jeopardized by the absence of available external reference points. To overcome this limitation, a method for performing an automatic selection of reliable natural tie-points from repeat-pass InSAR time-series, by exploiting persistent scatterers (PS) candidates, has been developed in the frame of the AlpSnow project and was presented in (Gonzalez et al., 2024), demonstrated by utilizing exemplary Sentinel-1 and TanDEM-X data.

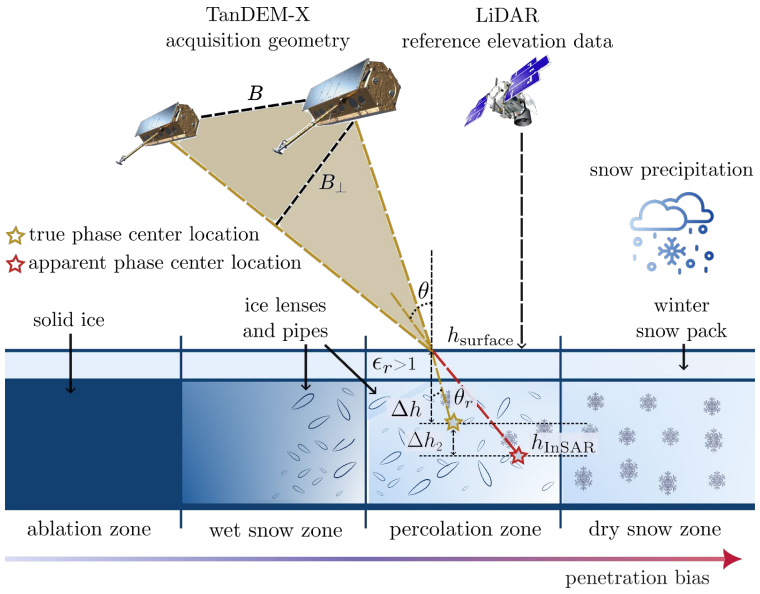

Figure 3.13: Schematic representation for deriving the surface height error as in Benedikter et al., 2023 for the bistatic TanDEM-X system. Higher penetration depths are expected as we move from the ablation and wet snow to the dry snow zone.

Recent preliminary results over a limited area of the Aletsch Gletscher, Switzerland demonstrate that compensating TanDEM-X DEMs for penetration-induced biases can substantially improve snow depth retrievals, yielding an average 66% reduction in relative snow depth estimation error (Becker Campos et al., 2026).

4. GAPS AND SCIENTIFIC CHALLENGES OF CURRENT RETRIEVAL ALGORITHMS

4.1. Snow Melt Phases

Ground-based and airborne SAR observations demonstrate that radar backscatter in the frequency range between 5 and 20 GHz is highly sensitive to changes in snow surface conditions, including transitions between dry snow, wet snow, and refrozen surface crusts. These changes strongly affect the dielectric properties and surface roughness of the snowpack, resulting in pronounced variations in SAR backscatter.

A major limitation in detecting and characterizing snowmelt phases is their strong temporal variability, which is driven by rapidly changing meteorological conditions and solar illumination. Consequently, dense time series of SAR acquisitions are required to adequately capture melt–refreeze dynamics. In alpine regions, snow surface conditions can evolve on sub-daily timescales due to diurnal melt–freeze cycles. Current satellite SAR systems are not able to fully resolve these rapid changes. For example, Sentinel-1 provides repeat-pass observations every six days using its two-satellite constellation, or approximately every 12 hours when considering ascending and descending orbits, but only on specific days. This temporal sampling is insufficient to continuously track sub-daily snowmelt dynamics.

To observe these rapid processes, new SAR system concepts with much higher temporal resolution, such as geostationary SAR (such as Earth Explorer 12 Candidate Hydroterra+), are required. In addition, the strong spatial variability of local incidence angles in mountainous terrain poses a further challenge, as it can significantly influence backscatter signatures and complicate the detection and monitoring of snowmelt phases.

In contrast, snowmelt and refreezing processes in polar regions are generally less dynamic on short timescales. There, daily to weekly SAR observations are often sufficient to monitor the onset of melt and the subsequent evolution of refreezing within the snowpack. Therefore, the development and validation of methods for detecting snowmelt phases and tracking the temporal evolution of refrozen crust thickness will initially focus on polar regions, such as the Antarctic Peninsula. These regions benefit from continuous coverage by existing C-band and L-band SAR satellite systems, providing an ideal testbed for methodological development before transferring the approaches to more dynamic alpine environments.

The developments and methods will be supported by numerical backscatter modelling and by applying an testing the methods on ground-based data sets with sub-daily data acquisitions.

4.2. Repeat-pass InSAR SWE retrieval:

Temporal decorrelation is a major source of error in repeat-pass InSAR SWE retrievals due to the fast-changing nature of snow. Even for relatively short temporal baselines of 6 days, coherence can decrease significantly for C- and L-band. The low coherence causes the image to contain high degree of noise, and heavy filtering is often required. Additionally, snow accumulation presents high spatial variability, often observing variations of 100 % within a few meters. These two effects complicate the accuracy of the retrieval as the heavy filtering required from the low coherence images, masks the spatial variability inherent in snow accumulation. Furthermore, high presence of noise can make successful phase unwrapping difficult. Techniques to reduce noise in the interferometric phase, while preserving the spatial structure of the snow are required for high spatial resolution retrievals. Coherence is commonly calculated using a boxcar-type

estimator, which assumes that the pixels within it are spatially stationary and represents the maximum-likelihood estimator of the InSAR coherence. Considering the high spatial variability of snow, this condition may not be fulfilled, with an increasing effect if large estimation windows are used to reduce noise and bias. Alternatives for it consist of e.g., adaptative networks (Vasile et al., 2006), or patch-wise non-local filters (Deledalle et al., 2010), which aim at providing a higher-resolution, denoised estimation of the interferometric phase and coherence. Additionally, MCh techniques and Maximum a Posteriori can provide alternatives to traditional InSAR workflows, where phase denoising and unwrapping are treated as different processes (Baselice et al., 2015).

Some of the current gaps in the retrieval of snow using ΔSWE using repeat-pass InSAR are:

- Temporal decorrelation is a strong limiting factor for high resolution retrieval, since it requires mitigation of noise through heavy filtering, often hindering spatial resolution. Snow accumulation often presents high spatial variability, which is lost in this process. Techniques preserving spatial feature could improve the accuracy of the retrievals.
- Phase unwrapping can be challenging in InSAR images with low coherence, even more if they present high spatial variability. For this reason, faulty unwrapping, leading to lost phase cycles, is relatively common in this application of InSAR (Belsinka et al., 2023; Benedikter et al., 2024).
- Changes in subnivean soil moisture induce an additional phase component which needs to be compensated (De Zan et al., 2013). During winter snow acts as an insulator and soil moisture remains relatively stable. However, during early season, when snow depth is small, liquid water resulting from melting of the upper layers can percolate to the soil, thus inducing an additional phase component.

4.3. Single-pass InSAR snow depth retrieval

Several methodological and scientific challenges remain for the accurate estimation of snow depth using single-pass InSAR:

- DEM-differencing approaches require effective compensation for radar penetration-derived biases. Recent studies have demonstrated the potential of data-driven bias correction strategies for TanDEM-X under varying InSAR acquisition geometries and snow conditions over the Greenland Ice Sheet (Becker Campos et al., 2026); however, these approaches require further validation and extension to more complex environments such as alpine glaciers and ice caps, as well as to other acquisition parameters (e.g. frequency, acquisition geometry).
- Long-term elevation changes assessments that combine DEMs from different missions, for example SRTM and TanDEM-X for multi-decadal glacier height change analyses (Rankl et al., 2016), encounter systematic discrepancies in elevation differences arising from distinct InSAR acquisition geometries, processing pipelines, and overall DEM quality.
- Progress in InSAR-based snow depth retrieval will depend on extending current methodologies beyond the X-band, particularly toward C- and L-band systems that will support forthcoming missions such as Harmony, ROSE-L, NISAR, and Sentinel-1-NG.
- The C- and X-band data acquired during the SRTM mission provide a valuable opportunity to transfer and adapt data-driven frameworks for X-band penetration-bias correction to C-band using fine-tuning or domain-adaptation strategies based on deep learning.

4.4. SWE from backscatter

Many of the challenges in relation to retrieving SWE from radar backscatter are common with passive microwave observations. These include:

- The spatial and temporal variability of snow microstructure affecting scattering intensity has been identified as one of the main impediments for accurate SWE retrievals from backscatter. Changes in microstructure may cause an equivalent or even larger change of the backscattering signal than increases in snow mass. Already for CoReH2O, assessments concluded that snow microstructure must be known a priori with a precision of +/- 15% in order to meet mission requirements (ESA2012). This can potentially be addressed by assigning retrieval priors based on physical snow process models predicting snow states, although this can lead to additional complications (Merkouriadi et al., 2020).
- Description of snow microstructure in physical scattering models. Two microstructure parameters are needed to fully characterize the microwave scattering of snow. The recently proposed microwave grain size (Picard et al., 2022) may offer a solution in this regard. However, this parameter is challenging to fully obtain from field observations, and is not directly simulated by physical snow process models.
- Dense forest cover remains and impediment to retrieving any surface properties using SAR. The response of vegetation transmissivity to freezing (Lemmetyinen et al., 2022) may enhance these possibilities but remains to be quantified and accurately represented in forward models of canopy scattering. Methods already derived for CoReH2O, which characterize forest scattering behaviour at local scales based on model fitting (Montomoli et al., 2015; Cohen et al., 2015) may offer a solution but remain to be tested over larger areas and different vegetation conditions/tree species.
- The snow background (i.e. ground) contribution to backscatter needs to be isolated from the snow volume contribution for retrieval of snow parameters. While the CoReH2O concept relied on a snow–free reference SAR acquisition to account for this component, it has been acknowledged that the ground scattering contribution during winter may differ from one measured prior to snowfall. Ground scattering will be affected by e.g. compaction of surface vegetation and changes in the soil permittivity due to freezing, and melt-refreeze crust formation at the snow-ground interface. The use of low frequency C- and L-band imagery to define the ground surface scattering properties has been proposed as a solution. However, the accuracy of present surface scattering models for transferring scattering properties across wavelengths needs to be validated for realistic winter conditions over diverse landscapes.

5. COORDINATION WITH OTHER RELEVANT PROJECTS AND ACTIVITIES

Table 5.1 summarizes key projects and activities from recent years, as well as those currently in progress. This activity will enable the exchange of information, facilitate access to reference and in situ data as well as ground-based, airborne, and satellite-based SAR datasets, and support the potential dissemination of advanced products generated within the SUPSAR-Snow project.

Table 5.1: Summary of other relevant projects and activities

Project	*Description*	*Time period*	*Web page*	*Contact person*
NASA SnowEx	Multiyear series of coordinated airborne remote sensing and field campaigns	2017, 2020, 2021, 2023	https://snow.nasa.gov/campaigns/snowex	Carrie Vuyovich
SNOWWI	Deployment of three-frequency airborne radar with interferometric capabilities	2023, 2024	https://science.nasa.gov/science-research/science-enabling-technology/technology-highlights/new-nasa-instrument-for-studying-snowpack-completes-airborne-testing/	Paul Siqueira, Hans-Peter Marshall
M³OCCA	International doctorate program conducting various in-situ measurement campaigns across glaciers in the European Alps	2022 -- 2030	https://www.idp-mocca.forschung.fau.de/	Matthias Braun
SUPSAR-IV	SUPSAR project on improving retrieval of ice velocity of ice sheets and glaciers.	2025-2027		Thomas Nagler
HYDROSWE	Multiyear timeseries of ground-based radar measurements of seasonal snow, with focus on C-band signal at high temporal resolution	2022-2025	NA	Juha Lemmetyinen
AlpSnow INARCH	Generation or snow products for more than 40 InARCH sites around the world	2024-2026	The INARCH sites provide dedicated in situ data on snowpack characteristics. Within the AlpSnow project, snow extent and albedo products derived from Sentinel-2 and Sentinel-3 are generated, together with wet snow products based on Sentinel-1 observations. New products developed within SUPSAR-Snow may also be of interest.	Thomas Nagler
SnowCCI	Generation of global SWE products	2026-2027	At present, snow water equivalent (SWE) products are primarily derived from passive microwave (PMW) data, which are not well suited for mountainous regions. SAR-based SWE products have the potential to fill this gap.	Thomas Nagler

6. TEST SITES FOR ALGORITHM DEVELOPMENT

Table 6.1 describes test areas selected for the project, including the main airborne and satellite datasets available. The main driver in test area selection was the availability of data.

Table 6.1: *Test areas for SUPSAR-Snow demonstration.*

Test site	*Characteristics*	*Main satellite and airborne datasets*	*Ancillary data*	*Parameters to be tested*
Sodankylä, Finland	Taiga/boreal forest	Sentinel-1, ALOS-2/4	Snow observation network (automated sensors for SWE and SD from several ecotypes) Manual snow observation program (weekly snow observations from main ecotypes) Monthly snow course observations (snow depth and SWE distriubution Tower-based radar observations from 9-17 GHz (forest clearing); 1-18 GHz (boreal forest stand) and 1-40 GHz (wetland)	SWE from repeat-pass InSAR SWE from multi-frequency microwave backscatter Snow melt processes from radar backscatter
Austrian Alps	Alpine	Sentinel-1, RCM, ALOS-2/4, TanDEM-X,, CosmoSkymed, SAOCOM, NISAR*	Dense network of automatic in situ meteo stations with snow height observations; manual snow pits;	SWE from repeat-pass InSAR Snow melt processes from radar backscatter Snow depth from DEM differencing
Antarctic ice sheet and shelves	Polar ice sheets / shelves	Sentinel-1, RCM, ASCAT, SAOCOM, ALOS-2/4, NISAR*, TerraSAR-X, TanDEM-X, BIOMASS*	-	Snow melt processes from radar backscatter
Trail Valley Creek, Northwest Territories, Canada	Tundra	Sentinel-1, RCM, ALOS-2/4, TanDEM-X, CryoSAR (L- and Ku-band)	Multi-year measurements of snow microstructure (layering, SSA), manual snow pits, bulk snow properties (SWE, SD).	SWE from repeat-pass InSAR SWE from multi-frequency microwave backscatter
Powassan, Ontario, Canada	Mid-latitude, agricultural	Sentinel-1, RCM, ALOS-2/4, TanDEM-X, CryoSAR (L- and Ku-band)	Winter 2022-2023 field campaign with measurements of bulk snow properties (SWE, SD), snow microstructure (layering, SSA), manual snow pits, soil status (freeze/thaw) and met observations.	SWE from repeat-pass InSAR SWE from multi-frequency microwave backscatter
Fortress, Alberta, Canada	Mid-latitude, mountain	Sentinel-1, RCM, ALOS-2/4, TanDEM-X, CryoSAR (L- and Ku-band)	Winter 2024-2026 field campaign with measurements of bulk snow properties (SWE, SD), snow microstructure (layering, SSA), manual snow pits, soil status (freeze/thaw) and met observations.	SWE from repeat-pass InSAR SWE from multi-frequency microwave backscatter

7. DATA SETS

7.1. Ground-based SAR experiments

While not being selected, CoReH2O provided the impetus for extensive field and modelling studies including acquisition of new radar datasets over seasonal snow and ice. The Nordic Snow Radar Experiment (Lemmetyinen et al., 2016) provided a four-season dataset (2009-2013) of near-continuous X-Ku band radar observations of boreal snow using the ground-based radar *SnowScat* (Werner et al., 2010). The measurements were used extensively to study forward models and retrieval concepts using radar backscatter.

Figure 7.1 summarizes the measured backscatter vs. in situ measured SWE during the first two seasons of NoSREx, comparing these for forward model simulations using MEMLS3Aa (Proksch et al., 2015). The measured average correlation length, a measure of the snow microstructure, was highly similar for these two seasons. Simulations results are shown with a +/- 20 % uncertainty in the correlation length. Subsequent seasons exhibited differing snow microstructural conditions and a differing sensitivity (see Lemmetyinen et al., 2016). Overall, the results demonstrate the differing response to SWE and snow microstructure of the two Ku band frequencies.

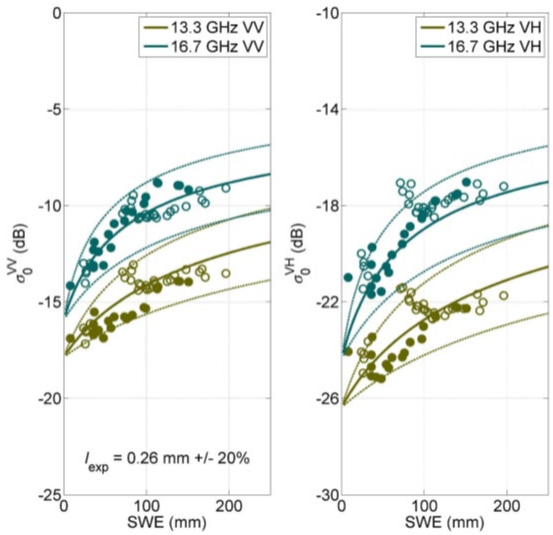

Figure 7.1: The relationship between SnowScat backscatter at 13.3 and 16.7 GHz and SWE for two seasons of the Nordic Snow Radar Experiment (NoSREx). Co-polarized VV (Left panel), cross-polarized VH (right panel). Blank symbols: 2009-2010; filled symbols: 2010-2011. Comparison to MEMLS3&a simulations (Proksch et al., 2015b) using measured correlation length +/- 20 %.

FMI has deployed the SodSAR ground-based SAR since 2018 for quasi-continuous measurements of radar backscatter over a boreal forest stand (Jorge Ruiz et al., 2020). The instrument is a stepped-frequency radar at four polarizations. The original instrument operated between 1-10 GHz; the radar was upgraded in 2022 to cover frequencies between 1-18 GHz. SodSAR includes a 3-axis positioner and a 5-m horizontal displacement rail, enabling SAR imaging. The instrument is mounted at a height of ca. 19 m overlooking a sparse forest consisting of mainly Scots pines; the imaged area also contains a non-vegetated area. The instrument acquires a SAR image of the test area typically every 6 hours. Ancillary data collection includes

sensors for measuring snow depth, SWE, soil temperature, soil moisture, and vegetation permittivity. Manual snow measurements (snowpits) have been conducted weekly at the site during winter periods. Data from the instrument has been applied to study the effect of environmental factors on decorrelation between SAR image pairs (Ruiz et al., 2022) and to examine the effect of temperature and snow on the canopy on attenuation of the radar signal in forests (Lemmetyinen et al., 2022).

The **ESA HydroSWE** (HydroSWE – Scatterometer Campaign and Data Analysis Study for Snow Water Equivalent Retrieval and GEO- and LEO-SAR Development) deployed the ESA WBSCAT instrument (Werner et al., 2019) in Sodankylä, Finland for three winter seasons. The instrument was deployed on a platform overlooking a wetland. Ancillary data collection includes snow depth, SWE, soil temperature and soil moisture from automated sensors. Manual snow measurements (stratigraphy, density, grain size etc.) were conducted weekly. The HydroSWE campaign was designed to analyse the potential to retrieve SWE at intervals of 1-12 days and identifying the limitations of SWE retrieval at these bands, which is relevant for missions like ROSE-L, Sentinel-1 and Hydroterra+. The analysis also covers investigations of coherence decay versus environmental factors such as snow accumulation rate, wind speed and temperature, and the investigation of synergies between L and C-bands for gap filling missed phase cycles. The project also includes an analysis of the measured multi-frequency time series of backscatter amplitude signatures at various bands (L, C, X, Ku-low, Ku-high, Ka) and polarizations (co- and cross-pol) over full winter periods. This aims to study the response of backscatter to changing physical snow parameters such as snow height, SWE, melt, liquid water content, and changing ground conditions. Finally, the study investigates the capabilities for retrieving freezing depth using combined C- and L-band data, which is relevant for Sentinel-1, Sentinel-1 Next Generation, and ROSE-L missions. Overall, the HydroSWE goals and dataset will contribute to the SUPSAR-Snow project.

7.2. Airborne experiments

7.2.1.SnowSAR Campaign Finland, Austria, Canada

The ESA SnowSAR is a dual-frequency (X-band and Ku-band), dual-polarized (VV, VH) airborne SAR, developed as a demonstrator instrument for the CoReH2O mission (Coccia et al., 2017). During Phase A studies of CoReH2O, the instrument was used to conduct multiple airborne campaigns in Finland, Canada, and Austria (Lemmetyinen et al., 2022), aiming to collect X-band and Ku-band signatures in diverse snow regimes and snow conditions including the boreal forest, Alpine glaciers, and tundra. Airborne acquisitions were supported by ground data collection along the instrument footprint. The measurements highlighted the sensitivity of the radar response to different types of snow. A low sensitivity to SWE was observed in particular over tundra sites, where predicted sensitivity by single-layer backscattering models was not reproduced in the observations (Figure 7.2). The SnowSAR data have been further exploited in the development of forward models and retrieval algorithms for snow water equivalent (SWE) (Zhu et al., 2018; Santi et al., 2022). The data have enabled to study the impact of forest vegetation on the X- and Ku-band SAR signal (Cohen et al., 2015; Montomoli et al., 2016).

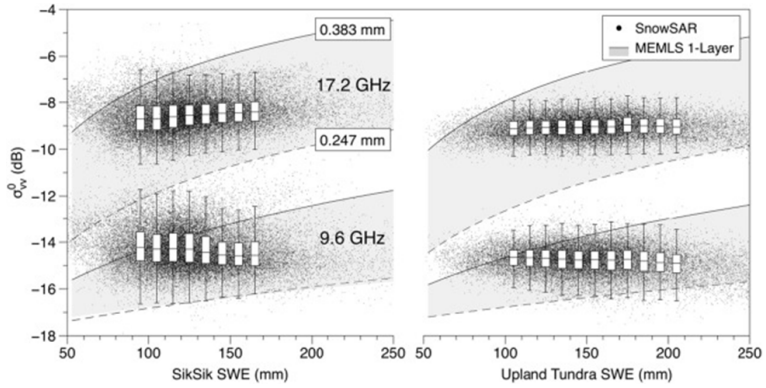

Figure 7.2: Relationship between SnowSAR σ_{vv}^0 and SWE at the SS and UT sites (black dots and boxplots). Grey shaded area shows the MEMLS 1-layer simulated range of variability based on snow pit measurements. The solid and dashed lines are for l_{ex} of 0.383 and 0.247 mm, representing the first standard deviation of measurements (King et al., 2018).

7.2.2. ESA SARSIM HT-NH – Airborne Campaign Wörgetal / Kühtai by ENVEO / DLR

F-SAR (*Flugzeug Synthetic Aperture Radar)* is an airborne SAR system developed and operated by the Microwaves and Radar Institute of the German Aerospace Center (DLR). F-SAR is typically operated on a twin-engine turboprop Dornier DO 228-212. The instrument supports five fully polarimetric frequencies at X-, C-, S-, L-, and P-bands; four bands can be operated simultaneously. F-SAR has been deployed for a campaign focusing on snow mass retrieval using InSAR over Wörgetal, Austria, in 2021. Dual polarization C- and L-band data were collected, together with supporting snow surveys on the ground performed by ENVEO.

7.2.3. Cryosphere-Observing SAR (CryoSAR) Campaign

The Cryosphere-Observing SAR (CryoSAR) system is a Ku- (13.5 GHz) and L-band (1.3 GHz) polarimetric SAR system designed to conduct observations of snow and ice on land and over water bodies, and soil moisture status (Kelly et al., 2024). Deployable from a small aircraft, CryoSAR has been used for several flight surveys over terrestrial, lake and sea ice sites between 2022-2025 (Figure 7.3). These data are available in the SUPSAR-Snow project through the University of Waterloo.

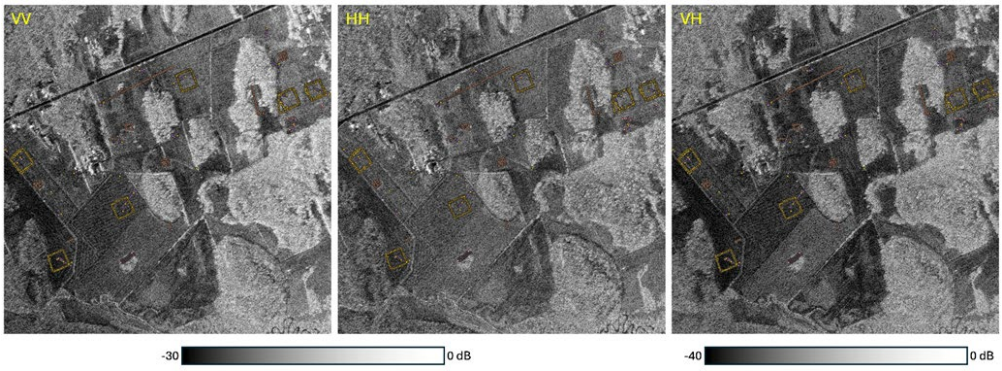

Figure 7.3: Example of airborne L-band CryoSAR data (VV, HH and VH polarization) from Powassan field site, Ontario, Canada on 3 March 2023. The superimposed data points are locations where magnaprobe snow depths were acquired during the campaign.

7.3. Summary of available datasets

Table 7.1 summarizes the datasets to be used in the SUPSAR-Snow project, including ground-based, airborne and satellite SAR datasets.

Table 7.1: Datasets available for SUPSAR-Snow.

Dataset	*Type*	*Availability*	*Characteristics*	*In situ data*
GROUND BASED DATA				
SodSAR	Ground-based SAR	Full dataset available from FMI	Continuous (6-12 hour repeat) ground-based SAR measurements at L-X band, 2018-present from boreal forest stand in Sodankylä, Finland.	Automated sensors (snow depth, SWE, AWS, soil properties, vegetation properties) Weekly Snow pits (stratigraphy, density, grain size, temperature, moisture profiles)
WBSCAT	Ground-based radar	Full dataset available via FMI. Instrument on loan from ESA	Continuous (3-6 hour repeat) radar observations at 1-40 GHz, winters of 2022-2023, 2023-2024 and 2024-2025. Wetland site in Sodankylä, Finland. Co-incident snow measurements.	Automated sensors (snow depth, SWE, AWS, soil properties, vegetation properties) Weekly Snow pits (stratigraphy, density, grain size, temperature, moisture profiles) Monthly snow course observations (snow depth and SWE distriubution
AIRBORNE DATA				
F-SAR	Airborne SAR	Available (ESA Campaign), provided by DLR	Snow Mass Campaign, Wörgetal/Küthai, Austria, 2021. C- and L-Band data, Dual polarization	Co-incident snow campaigns, available through ENVEO.
UAVSAR	Airborne SAR	Freely available. Distributed by NASA-JPL / NSIDC	Greenland and Alaska Campaigns, L-, P- and Ka-Band (2008 – present) Repeat-pass flights from NASA SnowEx test sites in Western US, 2020 and 2021.	Co-incident snow campaigns, available through NSIDC SnowEx database.
CryoSAR	Airborne SAR	Available through the University of Waterloo	Airborne L- and Ku-band quad-polarimetric SAR data from flight and field surveys over terrestrial, lake and sea ice sites 2022-2025. - Powassan, Ontario (terrestrial, agricultural): Dec 22, Mar. 2023; Nov. 23 – Jan. 24) - Inuvik/TVC, NWT (tundra) Apr. 24 (planned Mar. 25) - Cambridge Bay, Nunavut (tundra): Apr. 24 (and planned for Apr. 25). - Fortress Mountain, AB (alpine): Jan-Feb 25.	Ground correlative measurements acquired (build and microstructure).
SATELLITE DATA				
TanDEM-X	Spaceborne SAR Bistatic	The DLR investigators have full access to the global archive and commanding possibilities	Bistatic InSAR data at X-Band, StripMap mode 12 m resolution, HH polarization, global coverage (2010-present)	

Sentinel-1	Spaceborne SAR	Public, free	C-band Dual pol HH/VV and HV/VH, TOPS IWS, EW mode	
ICESat-2	Spaceborne LiDAR	Freely available. Distributed through the National Snow & Ice Data Center (NSIDC)	Six laser beams, global coverage, ground tracks (2018-present)	
NISAR	Spaceborne SAR	To be confirmed at a later stage of the project. Launch foreseen in 2025. Data will be made freely available by NASA	L-band SAR data. On-demand global coverage (future acquisitions)	
TerraSAR-X	Spaceborne SAR	Available through DLR	Powassan, Ontario, Canada. StripMap mode, VV/HH acquisitions over two swaths every 12 days, from October 2022- June 2023	campaign data on co-incident snow observations
RCM	Spaceborne SAR	Available through ECCC tasking. Data is available to all vetted users of RCM data (including international users).	Powassan, Ontario, Canada Fully polarimetric data acquired every 8 days from October 2022- June 2023 Ötztal, Austria Compact polarimetric (5m resolution) and fully polarimetric data. Many repeat passes have a four-day interval. Acquisitions started in October 2020 and is ongoing. Trail Valley Creek, NWT, Canada Compact polarimetric (5m resolution) and fully polarimetric data since January 2021.	campaign data on co-incident snow observations
ALOS-2 / 4	Spaceborne SAR	Available through ESA-JAXA collaboration agreement.	Time series from Sodankylä, Finland, HH/HV since 2019. 14-28 day repeat track (two orbits). Trail Valley Creek, NWT, Canada Fine Mode, HH/HV since July 2021 High sensitive mode full polarimetry since August 2021.	Sodankylä: Network of automated sensors (snow depth, SWE, AWS, soil properties, vegetation properties) Weekly Snow pits (stratigraphy, density, grain size, temperature, moisture profiles) Monthly snow course observations (snow depth and SWE distribution Canada: campaign data on co-incident snow observations

7.3.1.Auxiliary data

Dataset	*Type*	*Availability*	*Characteristics*
Copernicus DEM	Digital Elevation Model	Global coverage; static product with periodic updates Freely available	Global elevation data available at multiple spatial resolutions (e.g. 30 m and 90 m);
Copernicus Global Land Cover (GLC)	Discrete global land cover classification	Global coverage; annual or near-real-time products, freely available	Consistent worldwide classification scheme; spatial resolution of ~100–300 m;
Copernicus High Resolution Layers (HRLs)	Thematic land cover layers Global	European coverage; multi-annual updates (varies by layer)	High spatial resolution (10–20 m); derived mainly from Sentinel-1 and Sentinel-2 data; provides detailed information on specific land cover components (e.g. imperviousness, forests, grasslands, water and wetlands);

8. REFERENCES

Baghdadi, N., Bernier, M., & Gauthier, R. (1997). Capability of multitemporal ERS-1 SAR data for wet snow mapping. *Remote Sensing of Environment*, 60(2), 174–186. https://doi.org/10.1016/S0034-4257(96)00180-0Baselice, F.; Ferraioli, G.; Reale, D. Multi-frequency and multi-baseline ground-based SAR for environmental monitoring. *IWMN 2015* 2015, 1–5.

Becker Campos, A.; Braun, M. H.; Rizzoli, P. A snow properties-aware deep learning framework for large-scale estimation of penetration bias in TanDEM-X DEMs. *Kleinheubach Conference* 2025, 1–4.

Becker Campos, A.; Braun, M.; Rizzoli, P. A snow properties-aware deep learning framework for penetration bias estimation of TanDEM-X DEMs over ice sheets. *Remote Sensing of Environment, Accepted for publication,* 2026.

Belinska, K.; Fischer, G.; Hajnsek, I. Combining Differential SAR Interferometry and Copolar Phase Differences for Snow Water Equivalent Estimation. *IEEE Geosci. Remote Sensing Lett.* 2024b, *21*, 1–5. https://doi.org/10.1109/LGRS.2024.3461229.

Belinska, K.; Fischer, G.; Parrella, G.; Hajnsek, I. The Potential of Multifrequency Spaceborne DInSAR Measurements for the Retrieval of Snow Water Equivalent. *IEEE Journal of Selected Topics in Applied Earth Observations and Remote Sensing* 2024a, 17, 2950–2962.

Benedikter, A.; et al. Toward Dry Snow Parameter Estimation by Simultaneous Multiple Squint Differential InSAR. *IEEE Transactions on Geoscience and Remote Sensing* 2024, 62, 1–15, Art. 4303515.

Benedikter, A.; Rodriguez-Cassola, M.; Prats-Iraola, P.; Krieger, G.; Fischer, G. On the processing of single-pass InSAR data for accurate elevation measurements of ice sheets and glaciers. *IEEE Transactions on Geoscience and Remote Sensing* 2023, 62, 1–10.

Bonnell, R.; McGrath, D.; Tarricone, J.; Marshall, H.-P.; Bump, E.; et al. Evaluating L-band InSAR snow water equivalent retrievals with repeat ground-penetrating radar and terrestrial lidar surveys in northern Colorado. *The Cryosphere* 2024, 18, 3765–3785.

Braun, M. H.; Malz, P.; Sommer, C.; Farías-Barahona, D.; Sauter, T.; et al. Constraining glacier elevation and mass changes in South America. *Nature Climate Change* 2019, 9, 130–136.

Caves, R., Turpin, O., Nagler, T., & Mille, D. (1998). *The Role of Earth Observation in Snowmelt Runoff Monitoring from High Latitude Basins: SAR Aspects.* In Proceedings of the IEEE International Geoscience and Remote Sensing Symposium (IGARSS '98), Vol. 4, pp. 1858–1860.

Chang, W.; Tan, S.; Lemmetyinen, J.; Tsang, L.; Xu, X.; Yueh, S. H. Dense Media Radiative Transfer Applied to SnowScat and SnowSAR. *IEEE J. Sel. Top. Appl. Earth Observations Remote Sensing* 2014, *7* (9), 3811–3825. https://doi.org/10.1109/JSTARS.2014.2343519.

Coccia, A.; Trampuz, C.; Ortolani, M.; Turtolo, R.; Wieffering, T.; Meta, A. Deployment of the SnowSAR Sensor in the SnowEx Campaign by NASA and Preliminary Results. In *2017 IEEE International Geoscience and Remote Sensing Symposium (IGARSS)*; IEEE: Fort Worth, TX, 2017; pp 1403–1405. https://doi.org/10.1109/IGARSS.2017.8127227.

Cohen, J.; Lemmetyinen, J.; Pulliainen, J.; Heinila, K.; Montomoli, F.; Seppanen, J.; Hallikainen, M. T. The Effect of Boreal Forest Canopy in Satellite Snow Mapping—A Multisensor Analysis. *IEEE Trans. Geosci. Remote Sensing* 2015, *53* (12), 6593–6607. https://doi.org/10.1109/TGRS.2015.2444422.

De Zan, F.; Parizzi, A.; Prats-Iraola, P.; López-Dekker, P. A SAR Interferometric Model for Soil Moisture. *IEEE Transactions on Geoscience and Remote Sensing* 2014, 52, 418–425.

Deledalle, C.-A.; Denis, L.; Tupin, F.; Reigber, A.; Jäger, M. NL-SAR: A Unified Nonlocal Framework for Resolution-Preserving (Pol)(In)SAR Denoising. *IEEE Transactions on Geoscience and Remote Sensing* 2015, 53, 2021–2038.

Derksen, C., King, J., Belair, S., Garnaud, C., Vionnet, V., Fortin, V., Lemmetyinen, J., Crevier, Y., Plourde, P., Lawrence, B., Van Mierlo, H., Burbidge, G., Siqueira, P., 2021. Development of the Terrestrial Snow Mass Mission, in: 2021 IEEE International Geoscience and Remote Sensing Symposium IGARSS. Presented at the IGARSS 2021 - 2021 IEEE International Geoscience and Remote Sensing Symposium, IEEE, Brussels, Belgium, pp. 614–617. https://doi.org/10.1109/IGARSS47720.2021.9553496

Floricioiu, D., & Rott, H. (2001). Seasonal and short-term variability of multifrequency, polarimetric radar backscatter of alpine terrain from SIR-C/X-SAR and ERS-1. *IEEE Transactions on Geoscience and Remote Sensing*, 39(12), 2634–2648. https://doi.org/10.1109/36.975001

Gonzalez, C.; Dell'Amore, L.; Bueso-Bello, J.-L.; Milillo, P.; Schwaizer, G.; Nagler, T.; Rizzoli, P. Sentinel-1-Aided Mutual Calibration of TanDEM-X DEMs for the Estimation of Height and Volume Changes. *IEEE Journal of Selected Topics in Applied Earth Observations and Remote Sensing* 2024, 18, 3385–3397.

Guneriussen, T.; Hogda, K. A.; Johnsen, H.; Lauknes, I. InSAR for estimation of changes in snow water equivalent of dry snow. *IGARSS 2000 – IEEE International Geoscience and Remote Sensing Symposium* 2000, 2, 463–466.

Hensley, S.; Moller, D.; Oveisgharan, S.; Michel, T.; Wu, X. Ka-band mapping and measurements of interferometric penetration of the Greenland ice sheet by the GLISTIN radar. *IEEE Journal of Selected Topics in Applied Earth Observations and Remote Sensing* 2016, 9, 2436–2450.

Hoen, E. W.; Zebker, H. A. Penetration depths inferred from interferometric volume decorrelation observed over the Greenland ice sheet. *IEEE Transactions on Geoscience and Remote Sensing* 2000, 38, 2571–2582.

Hoppinen, Z.; Oveisgharan, S.; Marshall, H.-P.; Mower, R.; Elder, K.; Vuyovich, C. Snow water equivalent retrieval over Idaho – Part 2: Using L-band UAVSAR repeat-pass interferometry. *The Cryosphere* 2024, 18, 575–592.

Jorge-Ruiz, J. Enhancing Spatiotemporal InSAR Retrieval of Snow Water Equivalent Using Multichannel and MAP Estimators. In preparation.

Karbou, F., James, G., Fructus, M., & Marti, F. (2022). *On the evaluation of the SAR-based Copernicus Snow products in the French Alps.* Geosciences, 12(11), 420. https://doi.org/10.3390/geosciences12110420

Kelly, R.; Thompson, A.; Wang, W.; Akhavan, Z.; Welch, J.; Toose, P.; Derksen, C.; Montpetit, B.; Meta, A. The Airborne Cryospheric SAR System (CryoSAR): Characterizing Cold Season Hydrology Using Ku and L-Band Polarimetric SAR Observations. In *IGARSS 2024 - 2024 IEEE International Geoscience and Remote Sensing Symposium*; IEEE: Athens, Greece, 2024; pp 6559–6561. https://doi.org/10.1109/IGARSS53475.2024.10642350.

King, J. M. L., Kelly, R. E. J., & Thompson, A. (2019). *Sensitivity of Ku- and X-Band Radar Observations to Seasonal Snow in Ontario, Canada.* Canadian Journal of Remote Sensing, 45(6), 829–846. https://doi.org/10.1080/07038992.2019.1704621

King, J.; Derksen, C.; Toose, P.; Langlois, A.; Larsen, C.; Lemmetyinen, J.; Marsh, P.; Montpetit, B.; Roy, A.; Rutter, N.; Sturm, M. The Influence of Snow Microstructure on Dual-Frequency Radar Measurements in a Tundra Environment. *Remote Sensing of Environment* 2018, *215*, 242–254. https://doi.org/10.1016/j.rse.2018.05.028.

Krieger, G.; Moreira, A.; Fiedler, H.; Hajnsek, I.; Werner, M.; Younis, M.; Zink, M. TanDEM-X: A satellite formation for high-resolution SAR interferometry. *IEEE Transactions on Geoscience and Remote Sensing* 2007, 45, 3317–3341.

Lei, Y.; Shi, J.; Liang, C.; Werner, C.; Siqueira, P. Snow Water Equivalent Retrieval Using Spaceborne Repeat-Pass L-Band SAR Interferometry Over Sparse Vegetation Covered Regions. *IGARSS 2023 – IEEE International Geoscience and Remote Sensing Symposium* 2023, 852–855.

Leinss, S.; Antropov, O.; Vehviläinen, J.; Lemmetyinen, J.; Hajnsek, I.; Praks, J. Wet snow depth from TanDEM-X single-pass InSAR DEM differencing. *IGARSS 2018 – IEEE International Geoscience and Remote Sensing Symposium* 2018, 8500–8503.

Leinss, S.; Wiesmann, A.; Lemmetyinen, J.; Hajnsek, I. Snow Water Equivalent of Dry Snow Measured by Differential Interferometry. *IEEE Journal of Selected Topics in Applied Earth Observations and Remote Sensing* 2015, 8, 3773–3790.

Lemmetyinen, J., King, J., Derksen, C., Toose, P., Rutter, N., & Merkouriadi, I. (2018). *The influence of snow microstructure and vegetation on radar backscatter: airborne SnowSAR observations and modeling.* Remote Sensing of Environment, 215, 242–254. https://doi.org/10.1016/j.rse.2018.06.013

Lemmetyinen, J.; Cohen, J.; Kontu, A.; Vehviläinen, J.; Hannula, H.-R.; Merkouriadi, I.; Scheiblauer, S.; Rott, H.; Nagler, T.; Ripper, E.; Elder, K.; Marshall, H.-P.; Fromm, R.; Adams, M.; Derksen, C.; King, J.; Meta, A.; Coccia, A.; Rutter, N.; Sandells, M.; Macelloni, G.; Santi, E.; Leduc-Leballeur, M.; Essery, R.; Menard, C.; Kern, M. Airborne SnowSAR Data at X and Ku Bands over Boreal Forest, Alpine and Tundra Snow Cover. *Earth Syst. Sci. Data* 2022, *14* (9), 3915–3945. https://doi.org/10.5194/essd-14-3915-2022.

Lemmetyinen, J.; et al. Attenuation of Radar Signal by a Boreal Forest Canopy in Winter. *IEEE Geoscience and Remote Sensing Letters* 2022, 19, 1–5, Art. 2505905.

Lemmetyinen, J.; Kontu, A.; Pulliainen, J.; Vehviläinen, J.; Rautiainen, K.; Wiesmann, A.; Mätzler, C.; Werner, C.; Rott, H.; Nagler, T.; Schneebeli, M.; Proksch, M.; Schüttemeyer, D.; Kern, M.; Davidson, M. W. J. Nordic Snow Radar Experiment. *Geosci. Instrum. Method. Data Syst.* 2016, *5* (2), 403–415. https://doi.org/10.5194/gi-5-403-2016.

Liang, C.; Fielding, E. J. Measuring Azimuth Deformation With L-Band ALOS-2 ScanSAR Interferometry. *IEEE Transactions on Geoscience and Remote Sensing* 2017, 55, 2725–2738.

Luzi, G.; Noferini, L.; Mecatti, D.; Macaluso, G.; Pieraccini, M.; Atzeni, C.; Schaffhauser, A.; Fromm, R.; Nagler, T. Using a Ground-Based SAR Interferometer and a Terrestrial Laser Scanner to Monitor a Snow-Covered Slope: Results From an Experimental Data Collection in Tyrol (Austria). *IEEE Transactions on Geoscience and Remote Sensing* 2009, *47*, 382–393, doi:10.1109/TGRS.2008.2009994.

Malnes, E., Guneriussen, T., & Høgda, K. A. (2002). *Mapping of snow covered area with Radarsat in Norway.* Proceedings of IGARSS 2002, IEEE International Geoscience and Remote Sensing Symposium, Toronto, Canada, Vol. 2, pp. 808–810.

Manickam, S. S., & Barros, A. P. (2020). *A retrieval algorithm for wet snow using Sentinel-1 SAR time series.* Remote Sensing of Environment, 245, 111823. https://doi.org/10.1016/j.rse.2020.111823

Mätzler, C., 1987. Applications of the interaction of microwaves with the natural snow cover. Remote Sensing Reviews 2, 259–387. https://doi.org/10.1080/02757258709532086

Merkouriadi, I.; Lemmetyinen, J.; Liston, G. E.; Pulliainen, J. Solving Challenges of Assimilating Microwave Remote Sensing Signatures With a Physical Model to Estimate Snow Water Equivalent. *Water Resources Research* 2021, *57* (11). https://doi.org/10.1029/2021WR030119.

Moller, D.; Andreadis, K. M.; Bormann, K. J.; Hensley, S.; Painter, T. H. Mapping snow depth from Ka-band interferometry: Proof of concept and comparison with scanning LiDAR retrievals. *IEEE Geoscience and Remote Sensing Letters* 2017, 14, 886–890.

Montomoli, F.; Macelloni, G.; Brogioni, M.; Lemmetyinen, J.; Cohen, J.; Rott, H. Observations and Simulation of Multifrequency SAR Data Over a Snow-Covered Boreal Forest. *IEEE J. Sel. Top. Appl. Earth Observations Remote Sensing* 2016, *9* (3), 1216–1228. https://doi.org/10.1109/JSTARS.2015.2417999.

Montpetit, B.; King, J.; Meloche, J.; Derksen, C.; Siqueira, P.; Adam, J. M.; Toose, P.; Brady, M.; Wendleder, A.; Vionnet, V.; Leroux, N. R. Retrieval of Snow and Soil Properties for Forward Radiative Transfer Modeling of Airborne Ku-Band SAR to Estimate Snow Water Equivalent: The Trail Valley Creek 2018/19 Snow Experiment. *The Cryosphere* 2024, *18* (8), 3857–3874. https://doi.org/10.5194/tc-18-3857-2024.

Nagler, T. (1996). *Methods and analysis of synthetic aperture radar data from ERS-1 and X-SAR for snow and glacier applications.* PhD thesis, University of Innsbruck, Austria.

Nagler, T., & Rott, H. (2000). Retrieval of wet snow by means of multitemporal SAR data. *IEEE Transactions on Geoscience and Remote Sensing*, 38(2), 754–765. https://doi.org/10.1109/36.842004;

Nagler, T.; Rott, H.; Malcher, P.; Müller, F. Assimilation of Meteorological and Remote Sensing Data for Snowmelt Runoff Forecasting. *Remote Sensing of Environment* 2008, *112*, 1408–1420, doi:10.1016/j.rse.2007.07.006.

Nagler, T.; Rott, H.; Scheiblauer, S.; Horn, R.; Fischer, J.; Moreira, A.; Kubanek, J. Field Experiments for InSAR Retrieval of Snow Mass in Preparation for Copernicus ROSE-L. In Proceedings of the EUSAR 2024; 15th European Conference on Synthetic Aperture Radar; April 2024; pp. 110–113.

Nagler, T.; Rott, H.; Scheiblauer, S.; Libert, L.; Molg, N.; Horn, R.; Fischer, J.; Keller, M.; Moreira, A.; Kubanek, J. Airborne Experiment on Insar Snow Mass Retrieval in Alpine Environment. In Proceedings of the IGARSS 2022 - 2022 IEEE International Geoscience and Remote Sensing Symposium; IEEE: Kuala Lumpur, Malaysia, July 17 2022; pp. 4549–4552.

Oveisgharan, S.; Zinke, R.; Hoppinen, Z.; Marshall, H. P. Snow water equivalent retrieval over Idaho – Part 1: Using Sentinel-1 repeat-pass interferometry. *The Cryosphere* 2024, 18, 559–574.

Palomaki, R. T.; Sproles, E. A. Assessment of L-band InSAR snow estimation techniques over a shallow, heterogeneous prairie snowpack. *Remote Sensing of Environment* 2023, 296, 113744.

Pan, J.; Durand, M.; Lemmetyinen, J.; Liu, D.; Shi, J. Snow Water Equivalent Retrieved from X- and Dual Ku-Band Scatterometer Measurements at Sodankylä Using the Markov Chain Monte Carlo Method. *The Cryosphere* 2024, *18* (4), 1561–1578. https://doi.org/10.5194/tc-18-1561-2024

Proksch, M.; Mätzler, C.; Wiesmann, A.; Lemmetyinen, J.; Schwank, M.; Löwe, H.; Schneebeli, M. MEMLS3&a: Microwave Emission Model of Layered Snowpacks Adapted to Include Backscattering. *Geosci. Model Dev.* 2015, *8* (8), 2611–2626. https://doi.org/10.5194/gmd-8-2611-2015.

Rankl, M.; Braun, M. Glacier elevation and mass changes over the central Karakoram region estimated from TanDEM-X and SRTM/X-SAR DEMs. *Annals of Glaciology* 2016, 57, 273–281.

Rignot, E.; Jezek, K.; Van Zyl, J.; Drinkwater, M. R. Radar scattering from snow facies of the Greenland ice sheet: Results from the AIRSAR 1991 campaign. *IGARSS 1993 – IEEE International Geoscience and Remote Sensing Symposium* 1993, 1270–1272.

Rott, H., & Nagler, T. (1994). *Capabilities of ERS-1 SAR for snow and glacier monitoring in alpine areas.* In Proceedings of the 2nd ERS-1 Symposium: Space at the Service of Our Environment (ESA SP-361), pp. 965-970.

Rott, H.; Nagler, T.; Scheiber, R. Snow Mass Retrieval by Means of SAR Interferometry. *FRINGE 2003 Workshop* 2004, *550*, 29.

Rott, H.; Yueh, S. H.; Cline, D. W.; Duguay, C.; Essery, R.; Haas, C.; Hélière, F.; Kern, M.; Macelloni, G.; Malnes, E.; Nagler, T.; Pulliainen, J.; Rebhan, H.; Thompson, A. Cold Regions Hydrology High-Resolution Observatory for Snow and Cold Land Processes. *Proc. IEEE* 2010, *98* (5), 752–765. https://doi.org/10.1109/JPROC.2009.2038947.

Ruiz, J. J.; et al. Comparing InSAR Snow Water Equivalent Retrieval Using ALOS-2 With In Situ Observations and SnowModel Over the Boreal Forest Area. *IEEE Transactions on Geoscience and Remote Sensing* 2024, 62, 1–14, Art. 4302314.

Ruiz, J. J.; et al. Investigation of Environmental Effects on Coherence Loss in SAR Interferometry for Snow Water Equivalent Retrieval. *IEEE Transactions on Geoscience and Remote Sensing* 2022, 60, 1–15, Art. 4306715.

Ruiz, J. J.; Vehmas, R.; Lemmetyinen, J.; Uusitalo, J.; Lahtinen, J.; Lehtinen, K.; Kontu, A.; Rautiainen, K.; Tarvainen, R.; Pulliainen, J.; Praks, J. SodSAR: A Tower-Based 1–10 GHz SAR System for Snow, Soil and Vegetation Studies. *Sensors* 2020, *20* (22), 6702. https://doi.org/10.3390/s20226702.

Santi, E.; Brogioni, M.; Leduc-Leballeur, M.; Macelloni, G.; Montomoli, F.; Pampaloni, P.; Lemmetyinen, J.; Cohen, J.; Rott, H.; Nagler, T.; Derksen, C.; King, J.; Rutter, N.; Essery, R.; Menard, C.; Sandells, M.; Kern, M. Exploiting the ANN Potential in Estimating Snow Depth and Snow Water Equivalent From the Airborne SnowSAR Data at X- and Ku-Bands. *IEEE Trans. Geosci. Remote Sensing* 2022, *60*, 1–16. https://doi.org/10.1109/TGRS.2021.3086893.

Schellenberger, T., Ventura, B., Zebisch, M., & Notarnicola, C. (2012). *Wet snow cover mapping algorithm based on multitemporal COSMO-SkyMed X-band SAR images.* IEEE Journal of Selected Topics in Applied Earth Observations and Remote Sensing, 5(3), 1045–1053. https://doi.org/10.1109/JSTARS.2012.2190720

Sommer, C.; Malz, P.; Seehaus, T. C.; Lippl, S.; Zemp, M.; Braun, M. H. Rapid glacier retreat and downwasting throughout the European Alps in the early 21st century. *Nature Communications* 2020, 11, 3209.

Strozzi, T., & Mätzler, C. (1998). Backscatter measurements of snowpack characteristics at X- and Ku-band. *IEEE Transactions on Geoscience and Remote Sensing, 36*(3), 838–848. https://doi.org/10.1109/36.673681

Tan, S.; Chang, W.; Tsang, L.; Lemmetyinen, J.; Proksch, M. Modeling Both Active and Passive Microwave Remote Sensing of Snow Using Dense Media Radiative Transfer (DMRT) Theory With

Multiple Scattering and Backscattering Enhancement. *IEEE J. Sel. Top. Appl. Earth Observations Remote Sensing* 2015, *8* (9), 4418–4430. https://doi.org/10.1109/JSTARS.2015.2469290.

Thompson, A., & Kelly, R. E. J. (2021). *Considerations for Ku-Band Radar Retrieval of Snow Water Equivalent at Mid-Latitude Ontario Agricultural Sites.* Canadian Journal of Remote Sensing, 47(1), 119–142. https://doi.org/10.1080/07038992.2021.1898938

Tsang, L.; Durand, M.; Derksen, C.; Barros, A. P.; Kang, D.-H.; Lievens, H.; Marshall, H.-P.; Zhu, J.; Johnson, J.; King, J.; Lemmetyinen, J.; Sandells, M.; Rutter, N.; Siqueira, P.; Nolin, A.; Osmanoglu, B.; Vuyovich, C.; Kim, E.; Taylor, D.; Merkouriadi, I.; Brucker, L.; Navari, M.; Dumont, M.; Kelly, R.; Kim, R. S.; Liao, T.-H.; Borah, F.; Xu, X. Review Article: Global Monitoring of Snow Water Equivalent Using High-Frequency Radar Remote Sensing. *The Cryosphere* 2022, *16* (9), 3531–3573. https://doi.org/10.5194/tc-16-3531-2022.

Ulaby, F. T.; Stiles, W. H. The Active and Passive Microwave Response to Snow Parameters: 2. Water Equivalent of Dry Snow. *J. Geophys. Res.* 1980, *85* (C2), 1045–1049. https://doi.org/10.1029/JC085iC02p01045.

Vasile, G.; Trouve, E.; Lee, J.-S.; Buzuloiu, V. Intensity-driven adaptive-neighborhood technique for polarimetric and interferometric SAR parameters estimation. *IEEE Transactions on Geoscience and Remote Sensing* 2006, 44, 1609–1621.

Werner, C.; Suess, M.; Wegmuller, U.; Frey, O.; Wiesmann, A. The Esa Wideband Microwave Scatterometer (Wbscat): Design and Implementation. In *IGARSS 2019 - 2019 IEEE International Geoscience and Remote Sensing Symposium*; IEEE: Yokohama, Japan, 2019; pp 8339–8342. https://doi.org/10.1109/IGARSS.2019.8900459.

Werner, C.; Wiesmann, A.; Strozzi, T.; Schneebeli, M.; Matzler, C. The Snowscat Ground-Based Polarimetric Scatterometer: Calibration and Initial Measurements from Davos Switzerland. In *2010 IEEE International Geoscience and Remote Sensing Symposium*; IEEE: Honolulu, HI, USA, 2010; pp 2363–2366. https://doi.org/10.1109/IGARSS.2010.5649015.

Xiao, R.; Yu, C.; Li, Z.; He, X. Statistical assessment metrics for InSAR atmospheric correction: Applications to generic atmospheric correction online service for InSAR (GACOS) in Eastern China. *International Journal of Applied Earth Observation and Geoinformation* 2021, 96, 102289.

Yueh, S. H.; Dinardo, S. J.; Akgiray, A.; West, R.; Cline, D. W.; Elder, K. Airborne Ku-Band Polarimetric Radar Remote Sensing of Terrestrial Snow Cover. *IEEE Trans. Geosci. Remote Sensing* 2009, *47* (10), 3347–3364. https://doi.org/10.1109/TGRS.2009.2022945.

Zhou, J.; Lei, Y.; Pan, J.; Liang, C.; Zhang, Y.; Li, W.; Xiong, C.; Shi, J. Snow Water Equivalent Retrieval and Analysis Over Altay Using 12-Day Repeat-Pass Sentinel-1 Interferometry. *EGUsphere* (preprint) 2025.

Zhu, J.; Tan, S.; King, J.; Derksen, C.; Lemmetyinen, J.; Tsang, L. Forward and Inverse Radar Modeling of Terrestrial Snow Using SnowSAR Data. *IEEE Trans. Geosci. Remote Sensing* 2018, *56* (12), 7122–7132. https://doi.org/10.1109/TGRS.2018.2848642.